Journal of Naval Architecture and Marine Engineering
December, 2024
https://dx.doi.org/10.3329/jname.v21i2.74923 *http://www.banglajol.info*

NON-SIMILAR KELLER BOX ANALYSIS OF MAGNETO CHEMICALLY RADIATIVE BUONGIORNO'S NANOFLUID FLOWS PAST A STRETCHING SURFACE

Asra Anjum[1,2*], Shaik Abdul Gaffar[2], D. Sateesh Kumar[3], O. Anwar Bég[4], Samdani Peerusab[5]

[1*]Research scholar, Department of Engineering Mathematics, Koneru Lakshmaiah Education Foundation, Guntur, Andhra Pradesh,522302, India. Email: asraanjum84@gmail.com, Asra.Anjum@utas.edu.om
[2]Mathematics and Computing Skills Unit, Preparatory Studies Centre, University of Technology and Applied Sciences, Salalah, Sultanate of Oman. Email: abdulsgaffar0905@gmail.com; Abdulgaffar.Shaik@utas.edu.om
[3]Department of Engineering Mathematics, Koneru Lakshmaiah Education Foundation, Guntur, Andhra Pradesh,522302, India. Email: drsateeshdeevi@gmail.com
[4]Multi-Physical Engineering Sciences Group, Mechanical Engineering Department, Corrosion and Coatings Lab, Room 3-08, SEE Building, University of Salford, Manchester, M54WT, UK. Email: O.A.Beg@salford.ac.uk;
[5]Department of Engineering, University of Technology and Applied Sciences Salalah, Sultanate of Oman.
Email: samdanimohd82@gmail.com, Samdani.Peerusab@utas.edu.om

Abstract:

A non-similar Keller Box analysis of magnetochemically radiative Buongiorno's nanofluid flows past a stretched surface is presented in this work. It offers insightful information for raising the effectiveness of heat, and mass transmission. Numerous scholars have examined various topics, including radiation, porosity, aligned magnetic fields, mixed convection, and the Forchheimer number when including nanofluids in these flows. However, thermal radiation impact, chemical reaction, and magnetic parameters on Buongiorno's nanofluid through a stretching sheet do not yet have a mention within existing scholarly works. To fill in this knowledge vacuum and provide insightful information about these variables. The investigation uniquely encompasses coupled magnetic properties, chemical reactions, thermal radiation on heat, mass transmission in nanofluids, assimilating Brownian motion, buoyancy ratio, and thermophoresis, offering a comprehensive multi-physics analysis that was not previously explored. By employing the Keller Box method (KBFDM), after being converted into a set of nonlinear ODEs, from the PDEs that govern the flow analysis are solved numerically, MATLAB is utilized to obtain graphs and tabular values. The effects of elements without dimensions, such as heat radiation ($0 \leq R \leq 1$), chemical reaction ($0 \leq Kr \leq 5$), and magnetism parameter ($0 \leq M \leq 2$) on concentration, temperature, and velocity distributions are discussed. Additionally, Nusselt number, Sherwood number, and Skin friction impacts are demonstrated. Velocity depreciates with elevating magnetic parameters. The velocity field experiences a significant boost in response to rising thermal radiation and chemical reaction values. A greater magnetic field causes the concentration profile to rise steadily of nanoparticles. Moreover, as (Kr) raises steadily, velocity appreciates however, temperature and concentration diminish substantially. When the magnetic parameter (M) rises, the Schmidt number (Sc) and skin friction decay. Skin friction and Sherwood number show an upward trend for myriad increasing values of thermophoresis (Nt). The present study shows a compatibility rate of 99.9% with the previous research across different values of Nusselt (Nu) and Sherwood (Sh) numbers. Significantly, higher (Pr) enhances (C_f) and (Sh) because of thicker thermal and thinner momentum boundary layers, while decreasing the (Nu) to inhibit heat transfer. It is noteworthy that, increasing (Sc) elevates (C_f), (Nu) and (Sh) by enhancing fluid viscosity and reducing mass diffusivity, which causes concentration within BL to thicken, and improves shear stress and heat transfer efficiency. Through this work, significant knowledge concerning how to Boost the productivity of chemical processing and thermal control mechanisms in magnetic, radiative environments involving nanofluids can be gained for industrial processes.

Keywords: Buongiorno's nanofluid model; stretching surface; Brownian motion; thermophoresis; skin friction; Nusselt number; Sherwood number; finite difference technique

1813-8535 (Print), 2070-8998 (Online) Received on: July, 2024

NOMENCLATURE:

B_0	*Constant transverse (radial) magnetic field*	*Sh*	*Mass transfer coefficient*
C	*Nanoparticle volume fraction*	*T*	*Temperature of the fluid*
C_f	*Skin friction coefficient*	*U*	*Velocity*
c_p	*Specific heat*	*V*	*Velocity vector*
D_B	*Brownian diffusion coefficient*	*u, v*	*Dimensionless velocity components in x, y directions respectively*
Dm	*Mass diffusion*	*x*	*Streamwise coordinate*
D_T	*Thermophoretic diffusion coefficient*	*y*	*Transverse coordinate*
E	*Electrical field vector*		***Greek Symbols***
F	*Non-dimensional steam function*	α_m	*Thermal diffusivity of Nanofluid*
Gr_x	*Local Grashof number*	β	*Volumetric volume expansion coefficient of fluid*
G	*Acceleration due to gravity*	τ	*The ratio of the effective heat capacity of nanoparticle to the heat capacity of the fluid*
K	*Thermal diffusivity*	σ	*The electric conductivity of a fluid*
Re_x	*Local Reynolds number*	η	*The dimensionless radial coordinate*
Kr	*Chemical reaction parameter*	μ_f	*Dynamic viscosity*
k_m	*Effective thermal conductivity*	ν	*Kinematic viscosity*
*k**	*The mean absorption coefficient*	θ	*Non-dimensional temperature*
M	*Magnetic parameter*	ρ_p	*the fluid density of nanoparticles*
R	*Radiation Parameter*	ξ	*Dimensionless tangential coordinate*
Nb	*Brownian motion parameter*	ψ	*Dimensionless stream function*
Nt	*Thermophoresis parameter*	ϕ	*Dimensionless concentration*
Nr	*Buoyancy ratio parameter*	σ^*	*The Stefan-Boltzmann constant*
Nu	*Local Nusselt number (cone surface heat transfer rate)*	ρ_f	*Density of fluid*
p	*Pressure*	ρC_p	*Effective heat capacity*
Pr	*Prandtl number*		***Subscripts***
q_r	*Radiative heat flux*	*w*	*Conditions at the wall (cone surface)*
Sc	*Schmidt number*	∞	*Free stream conditions*

1. Introduction

Non-similar solutions refer to cases where the flow fields cannot be described by a single set of dimensionless variables. The profiles of the flow fields vary in a more complex manner that does not allow for simple scaling or similarity transformations. The governing equations retain their full complexity and often require numerical methods or more advanced analytical techniques for their solution. Non-similar solutions can handle more complex and realistic flow scenarios as compared to similar solutions. It provides detailed information about the flow fields without assuming any simplifications inherent in similarity transformations. Non-similar solutions are utilized in complex fluid dynamics problems where the flow features change

significantly concerning space and time, such as turbulent flows, separated flows, and flows around complex geometries. Examples include turbulent boundary layers, flow around bluff bodies, and flow with significant spatial or temporal variations. The complexity of the problem is suitable for cases where the flow does not exhibit self-similarity and requires more detailed analysis. Because of their large range of uses, non-similar boundary layer investigations are more significant both theoretically and practically. Non-similar modelling is an extremely effective tool. Non-similarity might arise because of several factors, including changes in free flow velocity, and heated wall fluctuations, Yu and Sparrow (1971) examined suction impact created by fluid infusion upon outer layer transfer of mass. Razzaq and Farooq (2021) investigated non-similar boundary layer flow along linear stretching surfaces. Their study encompasses various fluid models, providing a detailed exploration of the distinct flow patterns observed under different fluid model conditions. Jan *et al*. (2022) focused on the non-similar analysis of dissipative MHD Sisko nanofluid through a vertical surface with a heat source/sink using the BVP4c technique. Riaz *et al*. (2023) approximated the numerical solution for ternary hybrid nanofluid applying a non-similar methodology. By utilizing the local non-similarity technique, dimensionless coordinates are created from physical coordinates. Sagheer *et al.* (2024) investigated the process for reproducing dimensionless non-similar framework employing a localized non-similarity method to determine the effects of heat radiation, joule heating, viscosity dispersion, and magnetic and electric fields while taking Cu/water into account as a nanofluid. In their investigations, Farooq *et al*. (2024) examined the performance of a stretched surface with magnetized micropolar nanofluid flow, taking into consideration important variables like fluid dissipation and the source of heat.

Nanofluids have numerous applications, including food manufacturing, refrigeration units, heat pumps, and hybrid-driven motors. Nanotechnology is regarded as one of the most crucial factors driving the next foremost industrial innovation of the modern era. It reflects the most significant high-tech breakthrough that is currently being investigated. It strives to manipulate matter's structure at the molecular level to achieve invention in almost every industry and public endeavor, including the life sciences, semiconductor preservation, transport, ecology, physical sciences, and general security. The minimum thermal conduction of typical heat-transfer fluids, including ethylene glycol, oil mixture, and water are used in improving the efficiency of many microelectronic systems. To address this constraint, there is a significant incentive to develop novel fluids to transfer heat with much-increased conductivity values to improve thermal properties. Effective thermal conduction of a fluid is greatly increased when nanoparticles are added which improves the transport of heat. Nanofluids have a particular property that distinguishes them from ordinary solid-liquid combinations including millimeter and/or micrometer-sized particles. Due to settling processes, such particles can clog equipment and cause a decline in pressure. Choi and Eastman (1995) demonstrated experimentally that the inclusion of any combination base fluid's apparent heat transfer capacity significantly increases whenever there are nanocrystals present.

Buongiorno's nanofluid refers to a type of nanofluid that has been engineered with enhanced heat transfer properties. Buongiorno's research focuses on utilizing nanofluid to enhance the efficiency of heat transfer in multiple contexts, including industrial process heat exchangers, managing temperatures in auto engines, and cooling systems in electronic devices, by blending base fluid with nanoparticles. This technology has the potential to revolutionize heat transfer systems by offering more efficient and compact solutions, leading to improved energy

efficiency and performance in various engineering applications. However, practical implementation and scalability are still areas of active research and development. Thermal analysis and Brownian movement of tiny fluid particles, as revealed by Buongiorno (2006), are referred to as the "Buongiorno nanofluid model". According to Lee *et al.* (1999), nanofluids possess exceptional qualities for transferring heat compared to regular fluids. The two-dimensional incompressible viscoelastic magneto nanofluid Buongiorno's model with convective fluxes was presented by Rasheed *et al.* (2021) using the BVPh2 algorithm, considering the impacts of absorbing heat and production. A trustworthy mathematical approach for the intricate interactions that take place whilst film boiling nanofluids at the vapor-liquid interface was presented by Yahyaee *et al.* (2024). They proved that when it comes to simulating the film boiling of nanofluids, the Continuous-Species-Transfer technique is more precise and efficient. Bhavani *et al*. (2024) examined nanofluids' ultrafast velocity, which is essential for a safe non-radiative design, and observed that the produced nano-coolants were stable, suggesting that they might be applied as coolants. Humane *et al.* (2023) studied the Buongiorno provides a simulation of the consequences of both temperature and solvent movement on a magneto-micropolar fluid in an inclined porous stretchy material. Heat, mass transport of an Ag-H2O nano-thin film passing through a porous medium was studied using a modified version of Buongiorno's model by Wang *et al*. (2023). The impact of the emission of heat in a square cavity filled with a uniformly porosity fluid-saturated porous media on non-Darcian natural convection was demonstrated by Mahapatra *et al*. (2012). Yuming Chu *et al*. (2021) studied Buongiorno's nanofluid system for movement in stretched discs with gyrotactic microorganisms incorporated.

A stretching sheet describes a surface in fluid dynamics that is continuously stretched, usually in a linear fashion, leading to the formation of a boundary layer in the fluid nearby. The behavior of mass transport, heat, and flow close to the surface are all studied in this situation. The stretching motion induces a velocity field in the fluid. Applications include polymer processing, cooling of metallic sheets, and coating processes. This model helps in understanding and optimizing industrial processes involving continuously moving surfaces. One of the core issues in fluid dynamics is the idea of stretching sheets, providing insights into BL theory, both heat, and mass transfer phenomena, and aiding in the design and optimization of industrial processes. A stretching surface has more classified stream matter about its assembly and form polymer extruder. Heat transfer in MHD Williamson nanofluid fluid flow over a non-linear stretching sheet has been investigated by Abbas *et al.* (2022). Additionally, Khechekhouche *et al.* (2021) investigated enhancements to collector cover and energy audit. Sajjad *et al*. (2020) focused on improving highly melted liquid. Gireesha *et al*. (2020) demonstrated the upward flow of Jeffrey nanofluid's nonlinear MHD radiation via a nonlinearly porous sheet. The non-similar examination of micropolar magnetized nanofluid flow on an expanded surface was studied by Farooq *et al*. (2024). The solution of the mixed convective heat transport flow over, the extending surface was numerically researched by Ellahi *et al*. (2018). Tlili *et al*. (2021) investigated the thermal transport of unstable MHD narrow-film flow. Varatharaj K. et al. (2024) investigated linear and nonlinear stretching sheets for improved heat, and mass transmission in Casson nanofluid containing activation energy.

Magnetohydrodynamics (MHD) is the study of the behavior of electrically conductive liquids in the presence of magnetic forces such as liquid metals and plasma. MHD investigates how fluid motion and magnetic fields interact, creating forces and currents that affect the fluid as

well as the field. Key concepts of MHD include the magnetic Reynolds number, induction, and Lorentz force. MHD finds applications in engineering, geophysics, and astrophysics, which help comprehend star phenomena, earth's core dynamics, and the MHD-based devices design, aerodynamic ejection of polymer sheets, tiny MHD motors, and geothermal power plants, subsurface water networks, reservoirs for oil, fluid metallic substances in liquid form, and energy storage plants. Comparative research on thermal transport for the MHD fluid subjected to radiation past a plane and a cylindrical region is presented by Rehman *et al*. (2022), and the results showed that the temperature domain is stronger for a cylindrical bottom. Razzaq *et al*. (2021) investigated a non-similar solution for MHD Maxwell fluid atop an extending sheet. Generalized differential quadrature methodology was developed by Usman Ashraf *et al*. (2022) to model the MHD peristaltic motion of blood-based nanofluid. The mathematical modeling for MHD effects on revolving enlarging disc circulation including the transport of heat analyzed by Ahmad *et al*. (2021). Hayat *et al.* (2017) analyzed the MHD stagnating point flow of a thyrotrophic fluid with non-uniform heat absorption generation. The study concentrated on transferring heat via a porous sheet that was contracting. Jan *et al.* (2022) investigated magnetized Sisko nanofluid, with an emphasis on the consequences of the dissipation of viscous fluid. Hussain *et al.* (2022) examined the ramifications of electromagnetically driven nanofluid radiative flow with a dense dissipation. Chu *et al.* (2020) study looked at non-Newtonian nanofluid flow with MHD properties of spreading Riga plate.

Thermal Radiation refers to the process through which matter releases heat energy in the form of electromagnetic waves due to its temperature. The energy balance and heat transport in fluid systems can be greatly impacted by this radiation, which is mostly in the infrared range. Thermal radiation is governed by Planck's law, Stefan-Boltzmann law, and Wien's displacement law. It is essential in fields where radiative heat transfer interacts with conductive and convective processes, such as atmospheric science, astrophysics, and thermal engineering. The regulation of heat transport is the primary purpose of thermal radiation. The influence of thermal radiation on heat flow is significant for systems operating at temperatures higher than room temperature when the radiation from heated walls and the fluid being used differs. The flow of an electrohydrodynamic nanofluid in a wavy permeability chamber with heat radiation was numerically investigated by Sheikholeslami *et al*. (2019) using the Control Volume Based Finite Element Method (CVFEM). The study's main finding was that for high permeability values of the porous medium, convection flow and transmission of heat are enhanced. Ramzan *et al*. (2019) investigated the effects of gyrotactic microorganisms in a thermal radiative nanofluid flow with both types of carbon nanotubes along an upward conical in a sponge medium. The influence of thermal energy on the flow of heat through vertically stretched sheets with open convection temperature-dependent production and absorption of heat in a medium with pores was examined by Turkyilmazoglu (2019). Exact closed-form solutions for the said problem are found. It is concluded that the heat transfer rate is enhanced for the sink and the opposite pattern is monitored for the source. The time-dependent rotational flow of nanofluid comprising dust particles and carbon nanotubes through the vertical extended surface with thermal radiation and Hall current in a Darcy- Forchheimer permeability media is studied by Bilal and Ramzan (2019) MATLAB software is used to resolve the question mathematically.

Chemical Reaction refers to the process in which chemical species within a fluid interact and transform into different substances, altering the fluid's composition and properties. These reactions can be exothermic or endothermic, impacting the fluid's temperature and flowing

properties. This study involves kinetic reaction, species transport, and energy exchange. Chemical reactions in fluid dynamics are crucial in domains including chemical processing, the combustion process, and environmental engineering, where fluid flow and chemical transformations are essential. Applications for the flow of fluids paired with chemical reactions are numerous and include procedures for dehydration, emulsions of oil and water, paper making, food manufacturing, the drying process, and crop destruction through freezing. Buongiorno model with viscosity dissipation along with chemical reaction, activation energy was analytically studied by Khan *et al*. (2020) on an endless horizontal plate situated between two second-grade nano liquids that change over time. A framework was developed by Seyedi *et al*. (2020) to evaluate chemical reactions and linear thermal energy on Eyring-Powell liquid in a squeezing deforming channel numerically. MHD third-grade nano liquid flow, time-dependent with activation energy's impacts, variable thermal conductivity, and bio-convection beyond an extended sheet was examined by Chu *et al*. (2020). Gireesha *et al*. (2019) demonstrate the effect of the Buongiorno model on a Casson fluid through a stretchable sheet absorbed with thermal non-linear radiation and activation energy. It has been noted that increasing non-linear radiative flux values improves heat transmission rate. More recent investigations are done by Seyedi *et al*. (2020), Rasheed *et al*. (2021), and Shahid *et al*. (2021).

The present investigation uses an analytical model to simulate the steady-state laminar boundary layer flow of magnetochemically radiative Buongiorno's nanofluid past a stretched surface. Its potential applications include the major improvement of thermal management in energy systems, electronic device cooling, and industrial cooling systems through a better understanding of fluid dynamics and heat transmission under complex situations. It can also enhance HVAC systems and maximize thermal protection in aircraft engineering, improving efficiency and performance in a variety of high-tech apps. The purpose of this research is to achieve greater efficacy. The resilient second-order realistic implicit finite differences Keller Box Approach is utilized for solving dimensionless non-linear boundary value problems involving the wall boundary and free stream constraints. Using previous special instances that have been documented in the literature, authentication is accomplished. Distributions of temperature, concentration, and velocity are shown through graphs. The research article addresses significant knowledge gaps by focusing on the analysis of non-similar flows using the Keller Box method, providing more accurate and applicable results for real-world scenarios compared to traditional self-similar solutions. By applying Buongiorno's nanofluid model, which considers Brownian motion and thermophoresis, to a stretching surface scenario, the study enhances comprehension of the dynamics of nanofluids under complex boundary conditions. It also investigates the interaction of radiative heat transfer, chemical processes, and magnetic forces on nanofluid flows, offering a comprehensive analysis that is often overlooked in previous research. Overall, the article seeks to provide practical insights for industrial and engineering applications involving stretching surfaces, significantly advancing heat transmission and the realm of dynamics of fluids. The investigation's innovative feature consists of its multiple new contributions over previous studies. This will add a great deal to our understanding of how nanofluids travel across stretching surfaces. The present research article endeavours to tackle the subsequent research inquiries:

- The use of the Keller Box method to analyze non-similar flows, providing more accurate results for practical applications.
- The integration of Buongiorno's nanofluid model with complex boundary conditions, including magnetic fields, chemical reactions, and radiative heat transfer.
- How much influence does the magnetic field have on the flow dispersion?
- How does the flow change when heat radiation occurs?
- How do thermal radiation and magnetic parameters respond to the Nusselt number?
- How does the Sherwood number affect the parameters on (*Pr), (Sc),* and *(Kr)* of the flow?

This article extensively examines these variables' combined influence on nanofluid flows, particularly in the context of a stretching surface. These aspects highlight the article's novelty and its significant contribution to advancing comprehension of heat transfer and fluid dynamics in more intricate and realistic situations.

2. Mathematical Model

In this article, we study the Buongiorno nanofluid's laminar, the steady-state boundary layer that flows through an expanding surface that is incompressible. Included are species buoyancy impacts as well as heat effects. In Fig. 1a the physical model is displayed, the gravitational acceleration (g) exerts its force downwards.

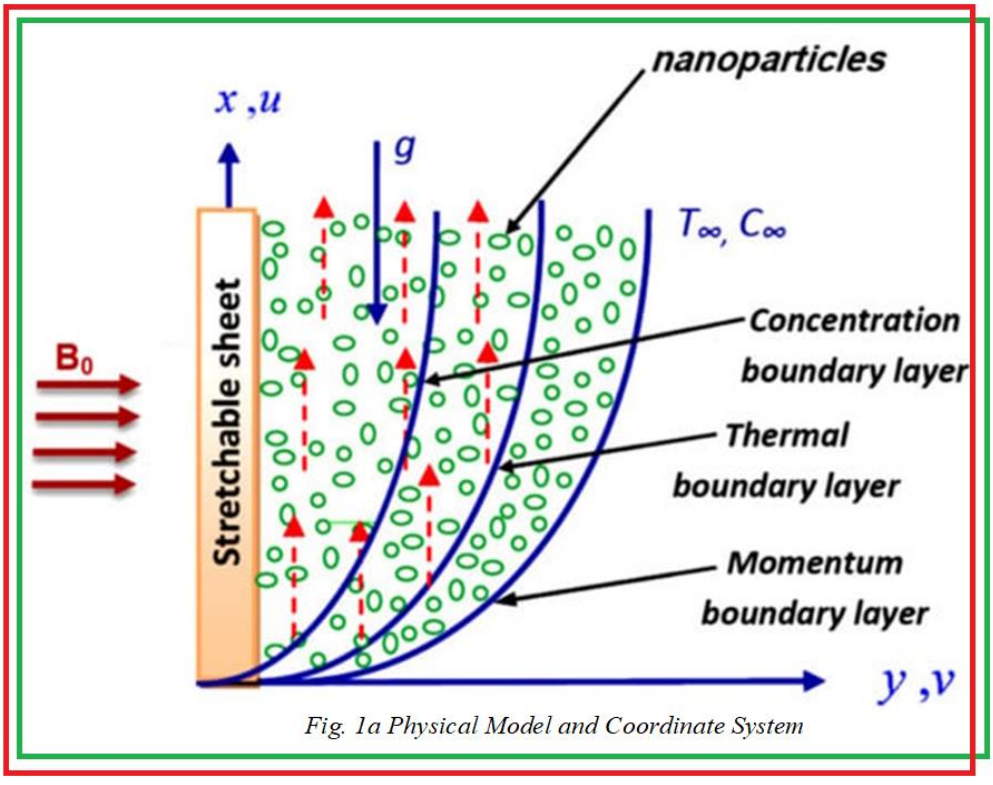

Fig. 1a Physical Model and Coordinate System

The governing equations for mass, momentum, energy, and nanoparticle species (concentration) for the Buongiorno nanofluid model (2006) under the boundary layer and Boussinesq approximations. They yield the following results:

$$\frac{\partial u}{\partial x}+\frac{\partial v}{\partial y}=0 \tag{1}$$

$$u\frac{\partial u}{\partial x}+v\frac{\partial u}{\partial y}=\nu\frac{\partial^2 u}{\partial y^2}+g\left[\beta\rho_{f\infty}\left(1-C_\infty\right)\left(T-T_\infty\right)-\left(\rho_p-\rho_{f\infty}\right)\left(C-C_\infty\right)\right]-\frac{\sigma B_0^2}{\rho}u \tag{2}$$

$$u\frac{\partial T}{\partial x}+v\frac{\partial T}{\partial y}=\alpha_m\frac{\partial^2 T}{\partial y^2}+\tau\left[D_B\frac{\partial T}{\partial y}\frac{\partial C}{\partial y}+\frac{D_T}{T_\infty}\left(\frac{\partial T}{\partial y}\right)^2\right]-\frac{\partial q_r}{\partial y} \tag{3}$$

$$u\frac{\partial C}{\partial x}+v\frac{\partial C}{\partial y}=D_B\frac{\partial^2 C}{\partial y^2}+\frac{D_T}{T_\infty}\frac{\partial^2 T}{\partial y^2}-K_1\left(C-C_\infty\right) \tag{4}$$

$$\text{Where } \alpha_m=\frac{k_m}{\left(\rho c\right)_f},\qquad \tau=\frac{\left(\rho c\right)_p}{\left(\rho c\right)_f} \tag{5}$$

The following pertinent boundary constraints are enforced in free stream and at the plate surface:

$$\begin{aligned} &u=u\left(x\right)=ax^m,\quad v=0,\quad T=T_w,\quad C=C_w,\quad at\quad y=0\\ &u\to 0,\qquad T\to T_\infty,\qquad C\to C_\infty,\qquad\qquad as\quad y\to\infty \end{aligned} \tag{6}$$

According to the Rosseland approximation, radiative flux is represented as follows.

$$q_r=-\frac{4\sigma^*}{3k^*}\frac{\partial T^4}{\partial y} \tag{7}$$

The following is how **T** can be broken down into a Taylor series for tiny temperature variations inside the flow:

$$T^4\cong 4T_\infty^3T-3T_\infty^4 \tag{8}$$

Equation (7) thus becomes:

$$q_r=-\frac{16\sigma^*T_\infty^3}{3k^*}\frac{\partial T}{\partial y} \tag{9}$$

Eqn. (1) is instantly fulfilled considering the subsequent velocity components defined in terms of stream function ψ :

$$u=\frac{\partial\psi}{\partial y}\quad and\quad v=-\frac{\partial\psi}{\partial x}.$$

The following dimensionless quantities are introduced:

$$\begin{aligned} &\xi=\frac{Gr_x}{\mathrm{Re}_x^2},\quad \eta=\frac{y}{x}\mathrm{Re}_x^{1/2},\quad \psi=\nu\,\mathrm{Re}_x^{1/2}\,f,\quad \theta\left(\xi,\eta\right)=\frac{T-T_\infty}{T_w-T_\infty}\\ &\phi\left(\xi,\eta\right)=\frac{C-C_\infty}{C_w-C_\infty},\qquad \mathrm{Re}_x=\frac{xu\left(x\right)}{\nu},\quad Gr_x=\frac{g\beta\left(T_w-T_\infty\right)\left(1-C_\infty\right)\rho_{f\infty}x^3}{\nu^2} \end{aligned} \tag{10}$$

Eqns. (2) - (4) are thereby rendered into the following coupled nonlinear ODEs:

$$f'''+\frac{1+m}{2}ff''-mf'^2+\xi\left(\theta-Nr\,\phi\right)-Mf'=\left(1-2m\right)\xi\left(f'\frac{\partial f'}{\partial\xi}-f''\frac{\partial f}{\partial\xi}\right) \tag{11}$$

$$\left(1+R\right)\frac{\theta''}{\mathrm{Pr}}+\frac{1+m}{2}f\theta'+Nb\,\theta'\phi'+Nt\,\theta'^2=\left(1-2m\right)\xi\left(f'\frac{\partial\theta}{\partial\xi}-\theta'\frac{\partial f}{\partial\xi}\right) \tag{12}$$

$$\frac{\phi''}{sc}+\frac{1+m}{2}f\phi'+\frac{1}{sc}\frac{Nt}{Nb}\theta''-Kr\phi=(1-2m)\xi\left(f'\frac{\partial\phi}{\partial\xi}-\phi'\frac{\partial f}{\partial\xi}\right) \tag{13}$$

The transformed non-dimensional boundary constraints are:

$$\begin{aligned} &f=0, \quad f'=1, \quad \theta=1, \quad \phi=1, \quad at \quad \eta=0 \\ &f'\to 0, \quad \theta\to 0, \quad \phi\to 0, \quad as \quad \eta\to\infty \end{aligned} \tag{14}$$

Here

$$\begin{aligned} &Nr=\frac{(\rho_p-\rho_{f\infty})(C_w-C_\infty)}{\rho_{f\infty}(1-C_\infty)\beta(T-T_\infty)}, \quad Nb=\frac{\tau D_B(C_w-C_\infty)}{\nu}, \quad Nt=\frac{\tau D_T(T_w-T_\infty)}{\nu T_\infty} \\ &\Pr=\frac{\nu}{\alpha}, \quad Sc=\frac{\nu}{D_m\varepsilon}, \quad M=\frac{\sigma B_0^2}{\mu\,\mathrm{Re}_x}, \quad R=\frac{16\sigma^* T_\infty^3}{3Kk^*}, \quad Kr=\frac{K_1x^2}{\nu\,\mathrm{Re}_x} \end{aligned} \tag{15}$$

The following definitions apply to the parameters used in engineering at the surface: skin-friction factor (C_f), which gauges shear stresses across the boundary along the *x-axis*; Sherwood number (*Sh*), which evaluates mass transmission rate; and Nusselt number (*Nu*), which assesses the temperature transmission rate.

$$\frac{1}{2}\mathrm{Re}_x^{1/2}C_f=f''(\xi,0) \tag{16}$$

$$\mathrm{Re}_x^{-1/2}Nu=-\theta'(\xi,0) \tag{17}$$

$$\mathrm{Re}_x^{-1/2}Sh=-\phi'(\xi,0) \tag{18}$$

3.1. Computational solution

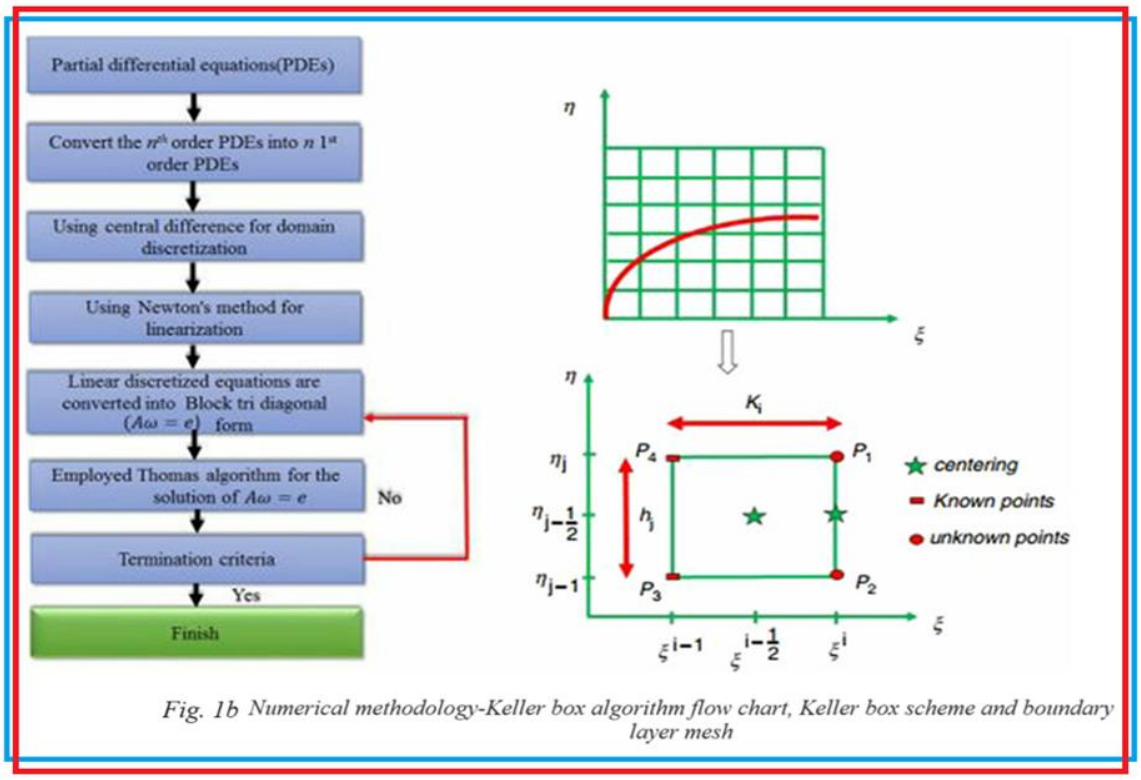

Fig. 1b Numerical methodology-Keller box algorithm flow chart, Keller box scheme and boundary layer mesh

The Keller box finite difference method (KBFDM) is employed to solve boundary layer (BL) problems in fluid dynamics. On a rectangular grid (*Fig. 1b*), a finite-difference technique is used ("box") and transforms PDEs into ODEs. This method ensures second-order accuracy and stability, making it effective for solving nonlinear boundary layer equations. It is particularly useful for problems involving complex geometries and varying boundary conditions, commonly applied in heat transfer and aerodynamics studies. (KBFDM) (1978), is considerably stronger and more efficient than many other computing approaches and yields second-order accuracy, is employed, and together with the boundary condition (14), to solve the dimensionless Eqns. (11) - (13) numerically. Vajravelu and Prasad (2014) have studied numerous uses of Keller's box approach in nonlinear nanofluid fluid dynamics. Prasad *et al*. (2014) conducted additional research on viscoelastic thermal axisymmetric coating fluxes, Gaffar *et al*. (2020) on thermal polymer coating flows of conical bodies; Basha *et al*. (2021) on entropy generation minimization in viscoelastic coating flows; Gaffar *et al*. (2014) on the boundary layer of thermal convection slip coating flow external to a spherical body; Gaffar *et al*. (2015) on magnetohydrodynamic non-Newtonian smart coating of wedge bodies with convective wall heating; Gaffar *et al*. (2024) on non-Darcy chemically radiative rotating flows; Gaffar *et al*. (2018) on Viscid Third-grade fluid passing over an isothermal overturned conical Gaffar *et al*. (2017) about Beyond the Newtonian Tangent hyperbolic liquid originating from a porous cone that is vertical; and Nasir *et al*. (2023) on bioconvection nanofluid flows in porous media saturated with oxytactic micro-organisms**.**

3.b. Validation of Keller box method

TABLE 1: COMPARATIVE RESULTS OF NUSSELT NUMBER AND SHERWOOD NUMBER FOR VARIOUS VALUES OF NT

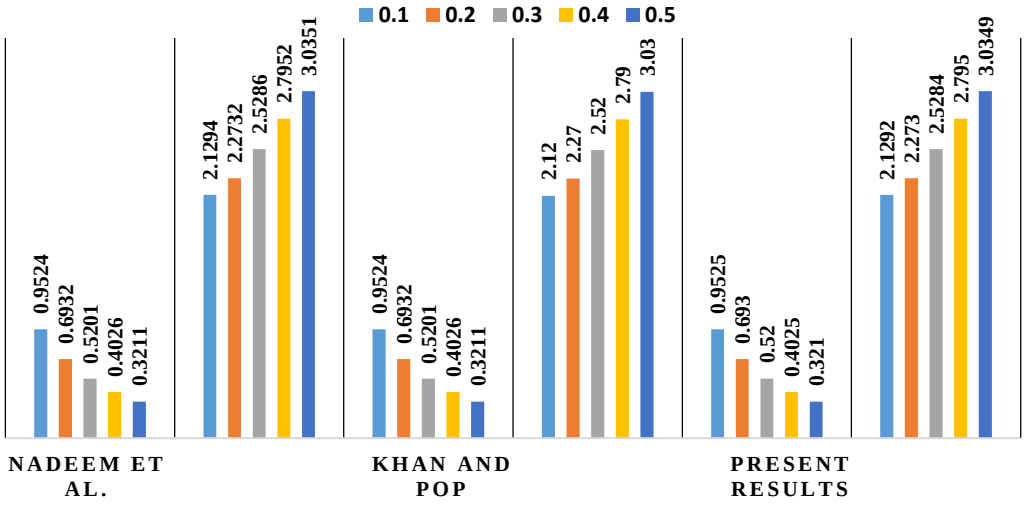

The Nusselt number (*Nu*) and Sherwood number (*Sh*) for (*Nt)* and ξvalues are compared to those published in the previous studies to assess the validity of the present numerical code. Table 1 shows this by comparing the validity of the current research to previous investigations by Nadeem *et al*. (2013), and Khan and Pop (2010). Based on the most recent results, there is

99.9% agreement with the conclusions. The data confirms that the present results validate and reinforce the findings of previous studies, indicating strong agreement and reliability in the observed trends.

4. Results and Discussion

This section emphasizes the physical viewpoint of a magneto chemically radiative Buongiorno's nanofluid flow through a stretching surface. (KBFDM) results of equations (11) - (13) are presented along radial coordinate (η) for figures and tables. These results of velocity (f'), temperature (θ), concentration (ϕ), as well as shear stress rate (C_f), heat transfer rate (Nu), nanoparticle mass transfer rate (Sh) for various values of the dimensionless thermophysical variables, namely the nanoparticle Brownian movement parameter (Nb), thermophoresis parameter (Nt), buoyancy ratio parameter (Nr), magnetic attraction parameter (M), thermal radiation parameter (R), and chemical reaction (Kr).

Figs. (2 – 11) provide a detailed graphical illustration of the velocity (f'), temperature (θ) and nanoparticle concentration (ϕ), skin friction (C_f), Nusselt number (Nu), and Sherwood number (Sh) distributions for different values of (Nb), (Nt), (Nr), (M), (R) and (Kr), the subsequent predefined values are applied to the parameters such as $Pr = 1$, $Nt = Nr = 0.3$, $Nb = 0.8$, $Sc = 0.6$, $m = 0.1$, $M = R = Kr = 0.5$ *and* $\xi = 1.0$ (unless otherwise stated). Here BL is (Boundary Layer).

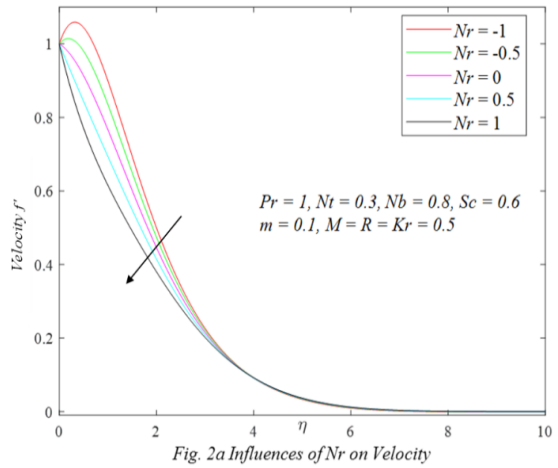

Fig. 2a Influences of Nr on Velocity

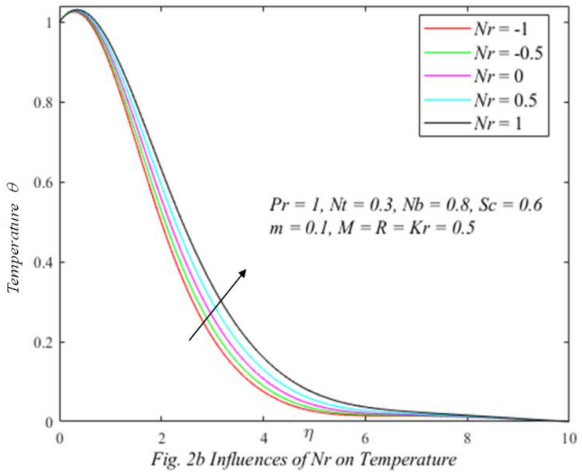

Fig. 2b Influences of Nr on Temperature

Figs. (2a – 2c) illustrate how the cumulative buoyancy ratio parameter, (Nr), affects (f'), (θ) and (ϕ) profiles throughout the BL regime. If $Nr < 0$, the forces of thermal buoyancy and species clash. If $Nr = 0$, forced convection occurs and buoyancy forces disappear. For $Nr > 0$, the buoyancy force helps the other. As seen in Fig. 2a, the velocity is suppressed with increasing (Nr). Physically, the growing buoyancy forces act against the flow, creating a resistance that slows it down. This opposing effect intensifies with a higher buoyancy ratio, reducing the overall velocity. Thus, the flow experiences greater deceleration as the buoyancy ratio parameter increases. The dual natural thermo-solute convection occurs, and the system displays buoyancy from both thermal and nanoscale components. Figs. 2b and 2c explore the patterns

exhibited by (θ) and (ϕ) profiles as we systematically increase the (Nr) values, and distinct changes become evident in the nanofluid dynamics. Notably, both (θ), and (ϕ) show an upward trend, signifying heightened internal buoyancy forces that improve heat, and mass transfer from surface to fluid. This results in higher thermal, solute gradients near the surface, causing increased (θ), and (ϕ) levels within BL. Physically, it signifies that stronger buoyancy effects lead to more efficient energy and species transport in the fluid. (f') converges to a value close to 1 for all values of (Nr). The convergence to this asymptotic value implies that beyond a certain point, further increases in η have minimal effects on (f'), it decreases as η reaches around 8 to 10. This suggests that the system reaches a steady state or equilibrium condition. All the curves eventually converge towards (θ) = 0 as η increases, showing that at a sufficient distance, temperature becomes negligible regardless of (Nr) values. (θ) increases monotonically and approaches 0 as η reaches around 8 to 10. (ϕ) increases monotonically and approaches 0 as η reaches 10. This augmentation enhances fluid motion, facilitating more effective mixing and transport of solute. This behavior highlights how the balance between thermal and solute buoyancy forces influences the distribution of concentration within the fluid.

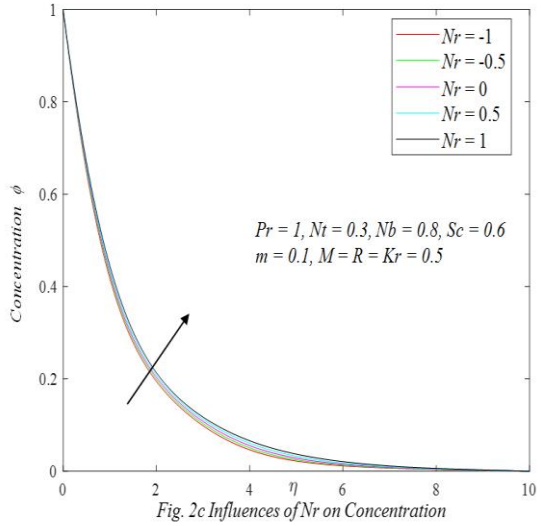

Fig. 2c Influences of Nr on Concentration

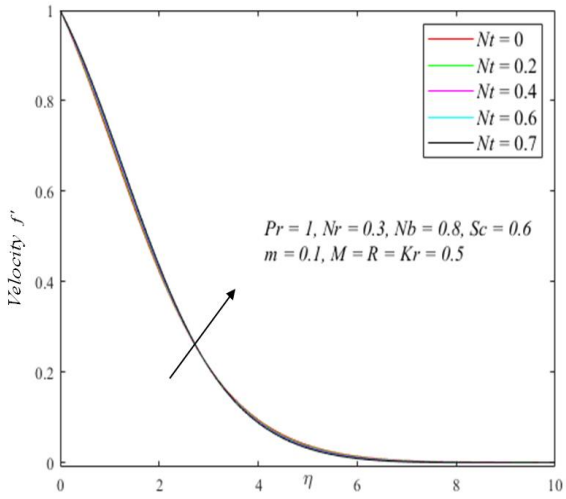

Fig. 3a Influences of Nt on Velocity

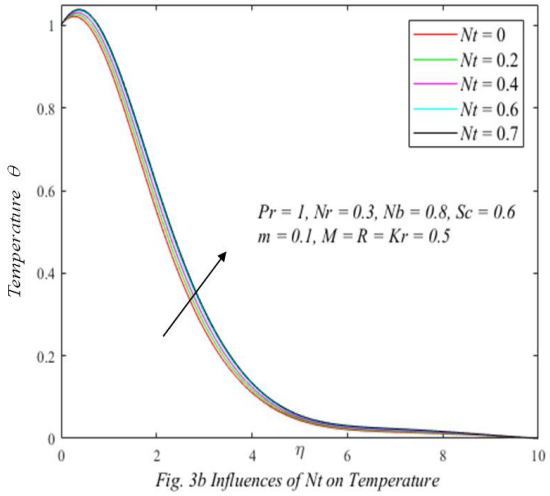

Fig. 3b Influences of Nt on Temperature

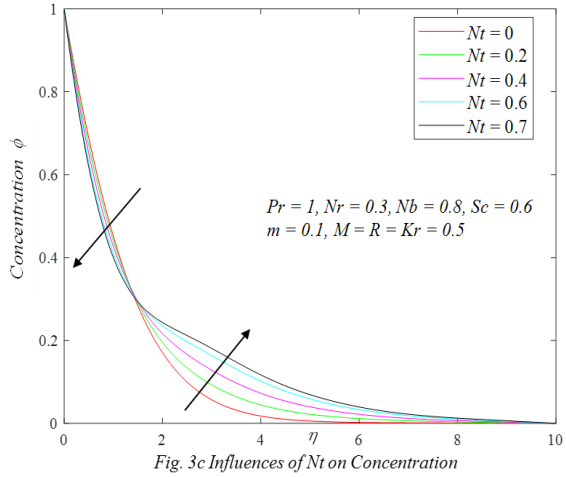

Fig. 3c Influences of Nt on Concentration

Figs. (3a – 3c) demonstrate how the thermophoresis parameter (*Nt*) affects (f'), (θ), and (ϕ) throughout the surface regime. Thermophoresis transports particles so that a temperature differential causes a fluid's temperature to compress. (θ), (ϕ) are significantly influenced by parameter *Nt*. When (*Nt*) increases, (f'), (θ) and (ϕ) profiles rise because of the increased migration of particles from hot to cold regions. This thermophoretic force contributes to the overall momentum transfer, thereby accelerating the velocity profile. Additionally, the increased movement of particles carrying heat away from the hot surface results in a higher temperature distribution within the fluid. As nanoparticles recede from the surface, the thermophoresis effect also contributes to an enhancement of the boundary layer's concentration profile. The volume percentage (ϕ) of nanoparticles firstly decreases and then takes a swirling turn and increases significantly as (*Nt*) improves because it worsens particle deposition away and enhances heat transport in the boundary layer and the fluid field. Physically, this signifies that a stronger thermophoretic force leads to enhanced momentum, heat, and mass transfer, reflecting more pronounced thermal and solutal gradients in the nanofluid flow. The two most intriguing aspects of Buongiorno's nanofluid model are thermophoresis and Brownian motion characteristics. In essence, these characteristics raise the fluid's temperature. The impact of a higher thermophoretic temperature gradient is significant on all transport characteristics, confirming the important role it plays in nanofluid mechanics. It is noteworthy that in Figs. (3a – 3c), the smooth convergence of all profiles in the free stream indicates that an appropriate large infinity boundary condition has been applied.

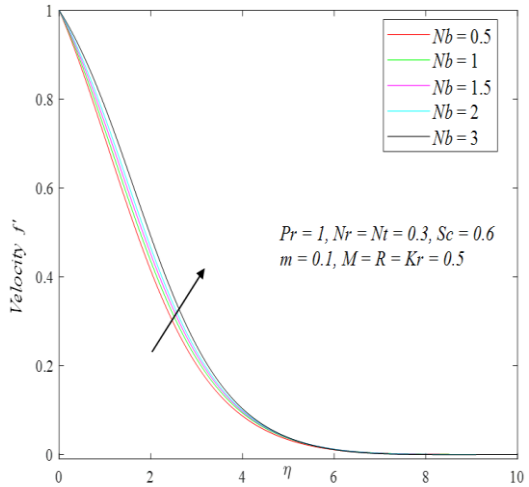

Fig. 4a Influences of Nb on Velocity

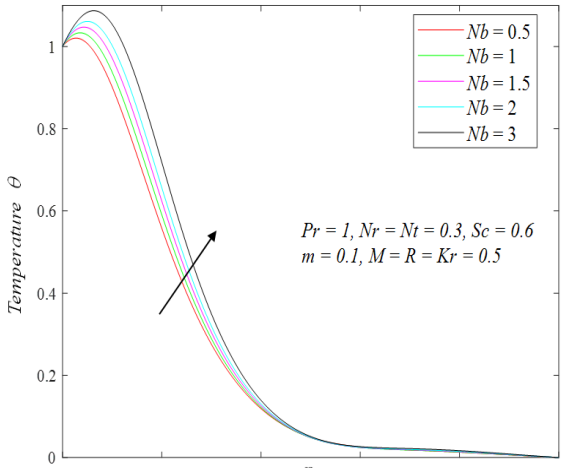

Fig. 4b Influences of Nb on Temperature

In Figs. (4a – 4c) we examine in detail the influences of Brownian motion (*Nb)*, on (f'), (θ), (ϕ) through the surface regime. The results show that variations in (*Nb)* have a discernible effect on the profiles. In Figs. (4a and 4b), as the *Nb* value steadily increases, a substantial and simultaneous elevation is observed in both (f') and (θ) graphs within the boundary layer. This suggests that augmenting the concentration of nanoparticles within the nanofluid results in increased fluid flow velocity and a higher temperature. The fundamental reason for this lies in heightened thermal conductivity and momentum transfer linked to a greater volume fraction of nanoparticles, thereby enhancing both heat transfer and fluid motion. However, from Fig. (4c), the concentration profile within the border layer shows a different pattern, which shows a discernible decrease with the enhancement of volume fraction. This observation can be

explained by considering the intensified interaction and agglomeration of nanoparticles. The physical significance of these observations lies in the complex interplay between Brownian motion and nanofluid dynamics. As the Brownian motion parameter increases, nanoparticles experience enhanced random movement, facilitating more efficient thermal diffusion and increasing fluid velocity. This phenomenon is crucial in applications requiring effective heat transfer, such as cooling systems and thermal management in engineering. However, the reduction in concentration gradient signifies a more homogeneous dispersion of nanoparticles, which can affect processes reliant on localized concentrations, such as drug delivery or materials synthesis. The fluid's Brownian motion is significantly impacted by increasing *Nb* levels because of the nanoparticles' random mobility. Furthermore, by gradually transferring nanoparticles from a hotter to a colder zone, thermophoresis boosts the temperature. It is noteworthy that in Figs. (4a – 4c) the smooth convergence of all profiles in the free stream indicates that an appropriate large infinity boundary condition has been applied.

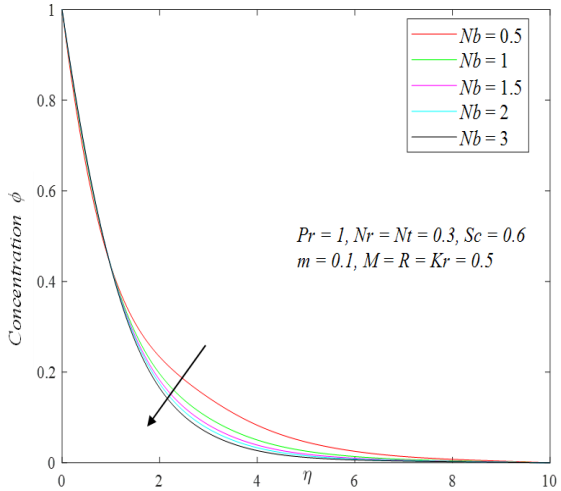

Fig. 4c Influences of Nb on Concentration

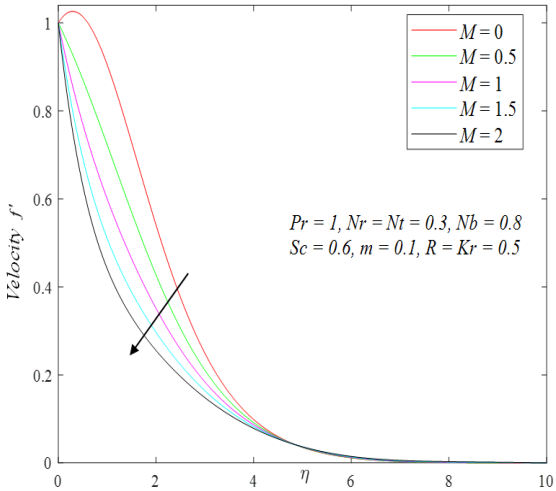

Fig. 5a Influences of M on Velocity

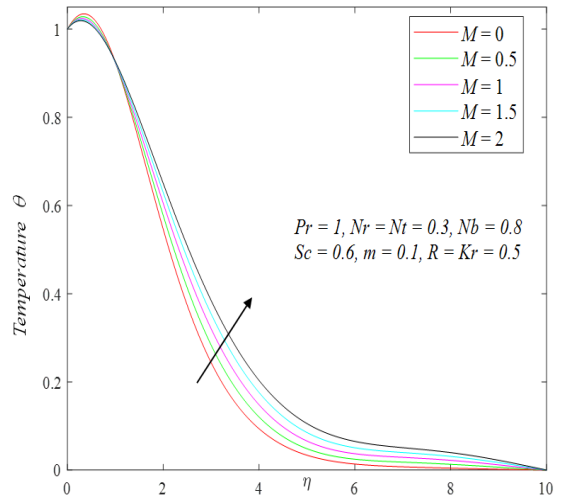

Fig. 5b Influences of M on Temperature

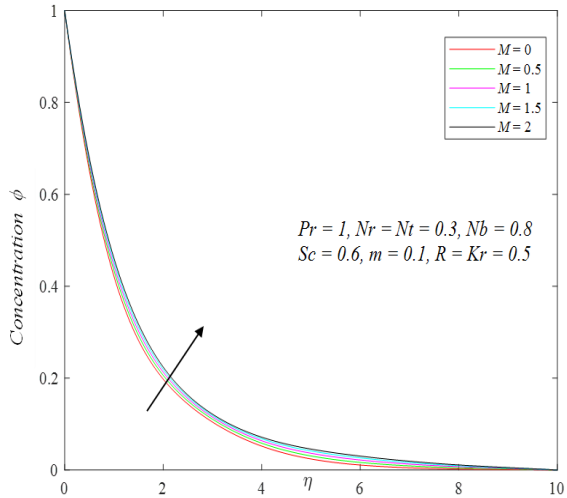

Fig. 5c Influences of M on Concentration

Figs. (5a – 5c) reflect a noticeable correlation as we enhance the values ($0 \leq M \leq 2$) which represent the magnetic parameter (M). From Fig. 5a, it is observed that (f') damps when (M) rises inside the boundary zone due to Lorentz force exerted on the conducting nanofluid. This

force acts contrary to the direction of flow direction, resulting in resistance that reduces fluid movement. Understanding this effect is crucial for applications in magnetohydrodynamics and fluid dynamics, where magnetic fields are used to control or manipulate fluid behavior, such as in magnetic drug targeting or magnetic fluid sealing technologies. From Figs. (5b and 5c) it is clear that as the (M) value steadily increases, a substantial elevation is witnessed in (θ) and (ϕ) profiles and is physically significant due to magnetic field-induced phenomena. Magnetic fields exert Lorentz forces on the conducting nanofluid, enhancing convective heat transmission and fluid movement close to a stretched surface. This leads to intensified thermal energy dispersion and enhanced transport of nanoparticles, resulting in elevated (θ) and (ϕ) nanoparticles in the boundary zone. These physical effects are crucial in applications such as magnetic drug targeting when exact control over temperature and particle distribution is vital for therapeutic efficacy and efficiency. (f') converges towards a similar asymptotic value (f') =1 as η increases, particularly beyond η≈8 approx. This suggests that the influence of the magnetic field becomes negligible far from the surface, where the flow reaches its free-stream velocity, and it decreases. Convergence of (θ) for different (M) values starts from (θ) =1 and converges towards (θ) = 0 as η increases, particularly beyond η≈10 approx. This indicates that far from the surface, the temperature of fluid approaches ambient temperature, and the influence of (M) on temperature diminishes. Convergence of (ϕ) from the graph shows that all curves for different (M) values converge as η increases, particularly around η≈10 approx. This indicates that at large distances from the boundary, the influence of (M) becomes negligible, and (ϕ) approaches the same asymptotic value (which is zero in this case).

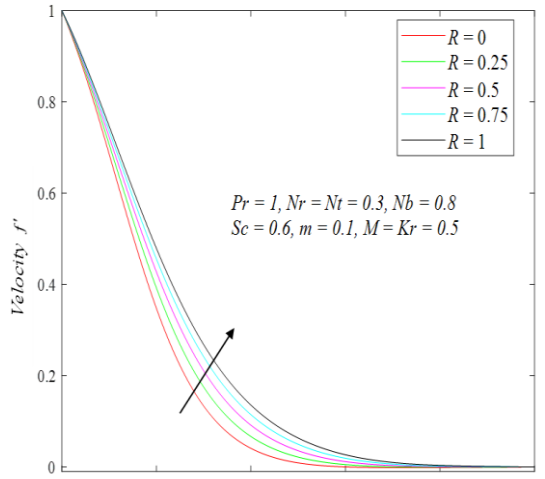

Fig. 6a Influences of R on Velocity

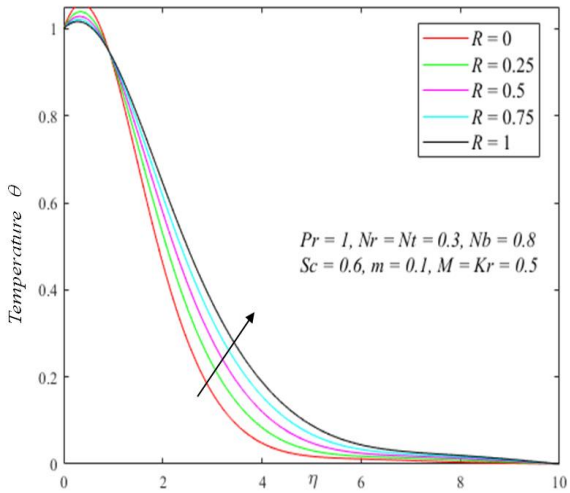

Fig. 6b Influences of R on Temperature

Figs. (6a – 6c) demonstrate the effects of *thermal radiation (R)* on $\left(f'\right)$, (θ) and (ϕ) surface regime. From Figs. (6a and 6b), we perceived that $\left(f'\right)$ and (θ) profiles are strongly accentuated for the values ($0 \le R \le 1$). Since the elevation of $\left(f'\right)$ and (θ) graphs with an increasing thermal radiation parameter are physically significant due to thermal radiation's role in thermal transmission mechanisms. As (R) rises, more heat is emitted and absorbed by the nanofluid, enhancing its thermal energy. This results in higher fluid velocities and temperatures near the stretching surface, influencing boundary layer dynamics and fluid flow characteristics. From

Fig. 6c the nanoparticle concentration dampens when the thermal radiation parameter increases due to enhanced thermal energy dissipation. Increased thermal radiation leads to more efficient heat transfer farther from the surface, reducing temperature gradients that drive nanoparticles, resulting in a more uniform distribution of nanoparticles throughout the fluid indicating more homogeneous dispersion throughout the fluid. Comprehending these physical consequences is crucial for enhancing heat transfer processes in numerous contexts where efficient thermal control is crucial, like solar thermal systems and electronic cooling. It is noteworthy that in Figs. (6a – 6c), the smooth convergence of all profiles in the free stream indicates that an appropriate large infinity boundary condition has been employed.

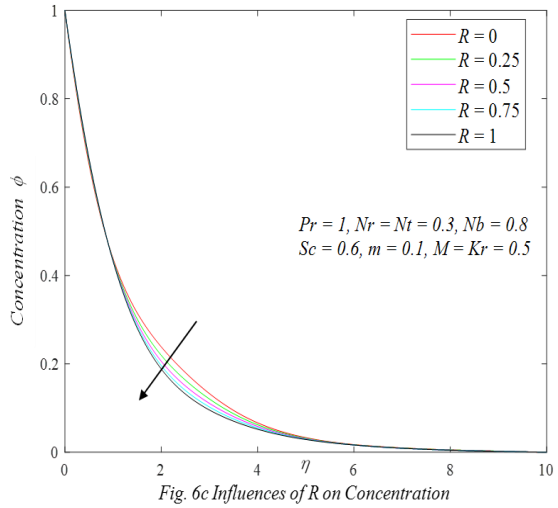

Fig. 6c Influences of R on Concentration

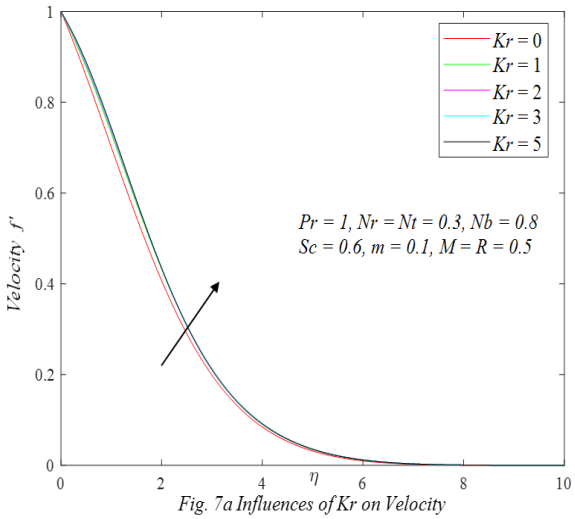

Fig. 7a Influences of Kr on Velocity

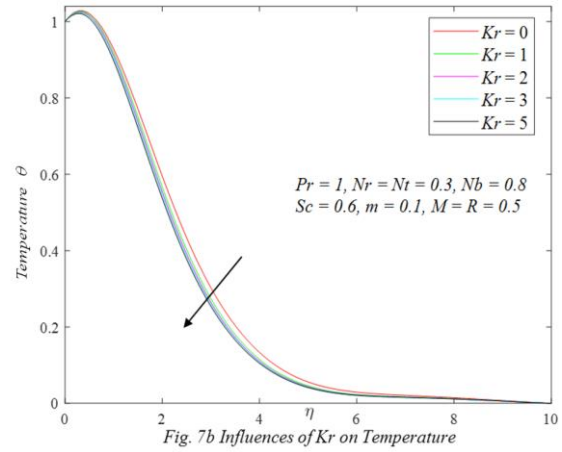

Fig. 7b Influences of Kr on Temperature

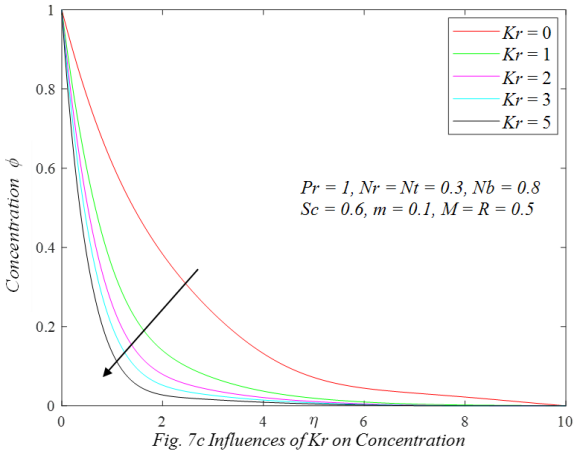

Fig. 7c Influences of Kr on Concentration

Figs. (7a – 7c) elucidate the effect of the chemical reactions *(Kr)* $(0 \le Kr \le 5)$ on (f'), (θ) and (ϕ) on boundary regime. From Fig. (7a) we detect that (f') rise steadily. The elevation of velocity with increasing chemical reactions is driven by multiple mechanisms. Chemical reactions in the nanofluid generate heat, alter fluid properties such as viscosity and density, and induce convective currents due to energy release or absorption. Additionally, these reactions can modify surface tension and interfacial properties, thereby influencing boundary layer dynamics and fluid velocities in the vicinity of the stretching surface. Figs. (7b and7c) depict that (θ) and (ϕ) profiles significantly depreciate the (θ) and (ϕ) profiles with an increasing chemical reaction parameter can be explained by several factors. Firstly, chemical reactions

often consume or release energy, altering the thermal energy balance within the nanofluid and potentially reducing overall temperature gradients. Secondly, changes in fluid properties due to chemical reactions, such as viscosity or density variations, can dampen convective heat and mass transport, leading to less pronounced concentration gradients of nanoparticles. Lastly, chemical reactions might affect nanoparticle aggregation or dispersion performance, influencing their distribution throughout the fluid and contributing to a more uniform concentration profile. Enhanced fluid motion is beneficial for applications requiring efficient mixing or transport, such as in chemical reactors or industrial processes. (f') converge towards a similar asymptotic value (f')=1 as η increases, beyond η≈ (6-8) approx. This suggests that the effect of chemical reaction becomes negligible far from the surface, where the flow reaches its free-stream velocity. Convergence of (θ) for different (*Kr*) values starts from (θ)=1 and converges towards (θ)=0 as η increases, particularly beyond η≈10 approx. This indicates that far from the surface, the temperature of fluid approaches ambient temperature. Convergence of (ϕ) from the graph shows that all the curves for different (*Kr*) values converge as η increases, particularly around η≈10 approx.

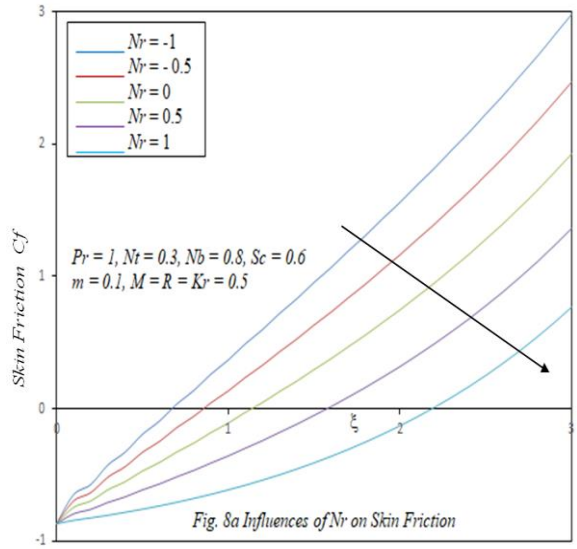

Fig. 8a Influences of Nr on Skin Friction

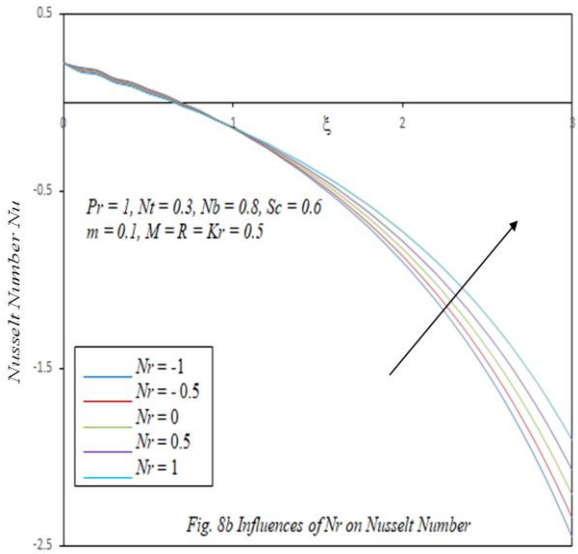

Fig. 8b Influences of Nr on Nusselt Number

Figs. (8a – 8c) indicate the buoyancy ratio parameter's *(Nr)* impact, (-1 ≤ *Nr* ≤ 1) on (C_f), *(Nu)*, and *(Sh)* along the surface regime. The decay in (C_f), (*Sh*) with an increasing *(Nr)* is attributed to the intensification of buoyancy forces opposing fluid motion. These forces reduce the shear stress at the surface, leading to lower (C_f). Additionally, the reduced *(Sh)* indicates reduced mass transfer rates due to hindered fluid movement caused by buoyancy effects. Conversely, the appreciation of *(Nu)* suggests enhanced heat transfer efficiency as the (*Nr*) increases. This occurs because stronger buoyancy forces augment convective heat transfer near the surface, improving the rapidity of exchange of heat energy between fluid and the stretching surface. Physically, these phenomena are significant in applications such as thermal management systems and heat exchangers, where controlling heat transfer rates and fluid dynamics is crucial. Understanding the impact of buoyancy on these parameters helps optimize the design and operation of such systems, ensuring efficient energy utilization and performance enhancement in various industrial and engineering contexts.

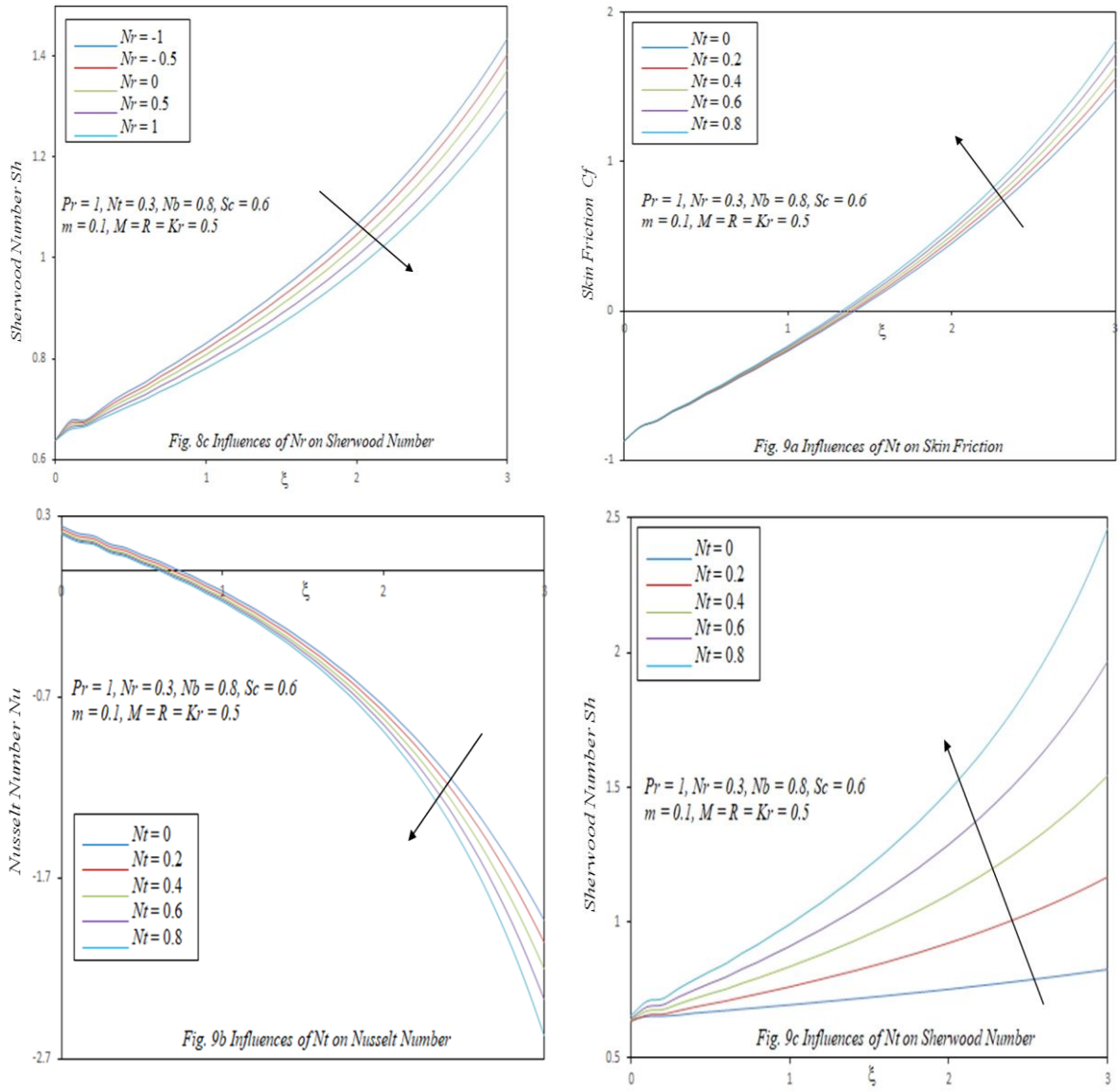

Figs. (9a – 9c) display the impact of *thermophoresis parameter (Nt),* ($0 \leq Nt \leq 0.7$) on, (C_f), *(Nu),* and *(Sh)* along the surface regime. Substantial rise in (C_f) and *(Sh)* as *(Nt)* rises, *is* primarily due to enhanced nanoparticle deposition near the surface. Thermophoresis induces nanoparticles to migrate towards regions of temperature gradient, leading to a higher deposition rate and subsequently increasing (C_f) and *(Sh)* rates. On the contrary, depreciation of (*Nu*) occurs because thermophoresis hinders convective heat transfer efficiency. Nanoparticles accumulating near the surface act as thermal barriers, reducing effective heat transport area and slowing down convective heat exchange between fluid and surface. Scientifically, these observations are significant in applications involving nanofluids, such as heat exchangers and thermal coatings. Understanding how thermophoresis affects these parameters helps in optimizing heat transfer processes and designing effective thermal management systems that regulate the deposition of nanoparticles, and dissipation of heat is critical for performance and operational efficiency.

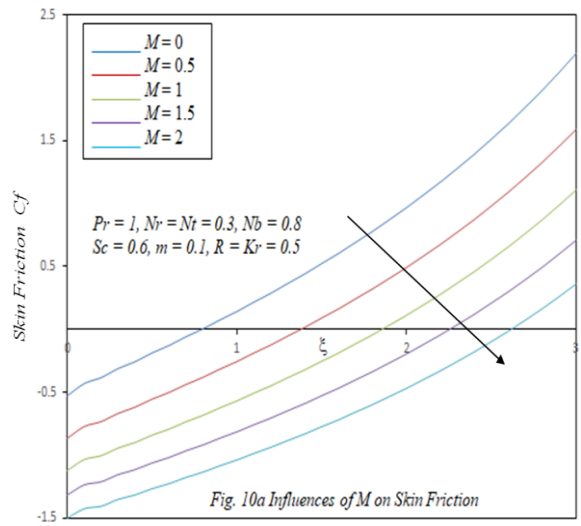

Fig. 10a Influences of M on Skin Friction

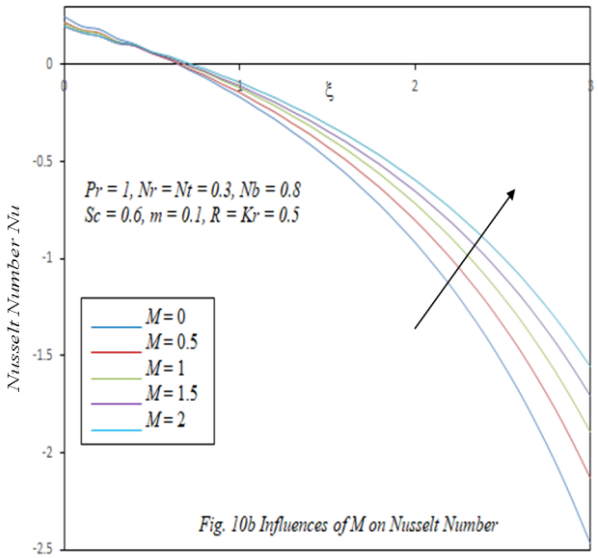

Fig. 10b Influences of M on Nusselt Number

Figs. (10a – 10c) elucidate the impacts of magnetic factor *(M)*, $(0 \leq M \leq 2)$ on (C_f), *(Nu)*, and *(Sh)* along the surface regime. The magnetic parameter's impact is profound and multifaceted. The decline in (C_f) and (*Sh*) arises from magnetic field-induced Lorentz forces, which diminish frictional resistance and reduce nanoparticle deposition near the surface, thereby lowering the Sherwood number. On the contrary, the magnetic field enhances (*Nu*) by intensifying convective heat transfer efficiency through increased fluid mixing and convective currents. This improvement signifies enhanced heat exchange between the nanofluid and the surface, crucial for applications like magnetic cooling systems and thermal management devices. These findings underscore the importance of understanding magnetic field effects for optimizing heat transfer and reducing energy losses in advanced nanofluid-based technologies across engineering and industrial sectors.

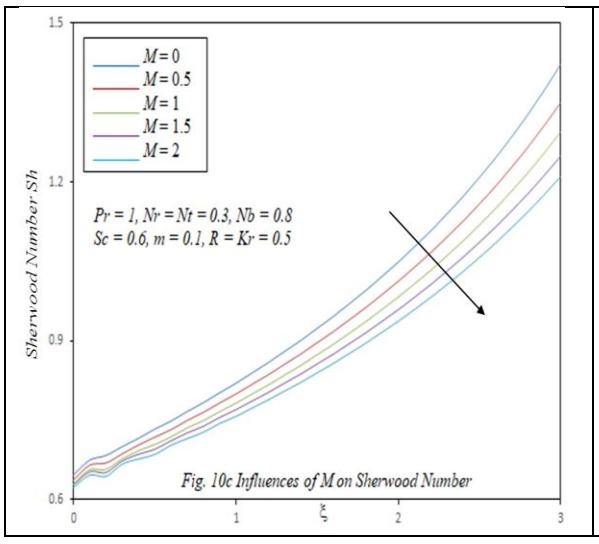

Fig. 10c Influences of M on Sherwood Number

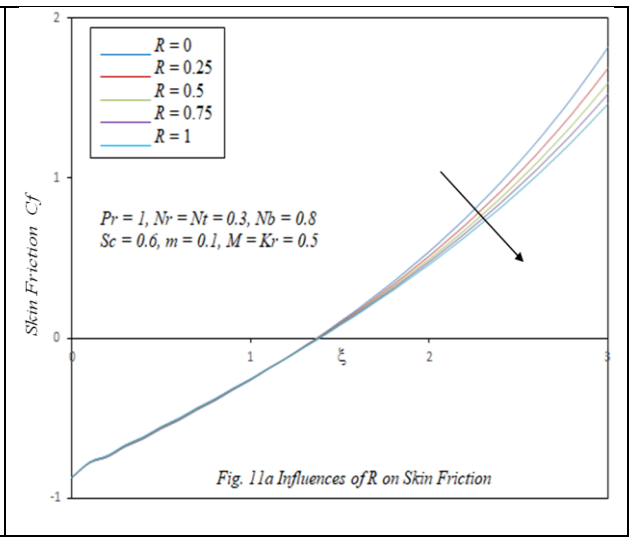

Fig. 11a Influences of R on Skin Friction

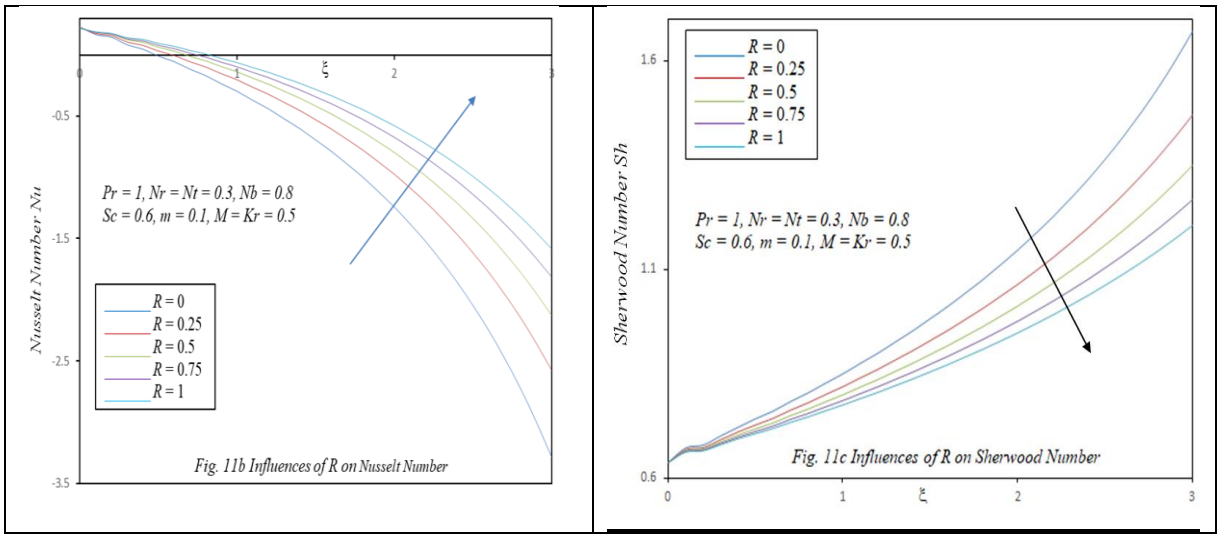

Figs. (11a – 11c) illustrate influences of thermal radiation parameter *(R)*, $(0 \leq R \leq 1)$, on (C_f), *(Nu) and (Sh)* along the surface regime. The depletion in *(Cf)* coefficient and (*Sh*) with an enhancing *(R)* is explained by enhanced heat transfer that occurs away from the substrate. As *(R)* rises, more thermal energy is radiated from the surface, reducing the temperature gradient and subsequently lowering (C_f), *(Sh).* However, appreciation of (*Nu*) occurs because elevated thermal radiation intensifies convective heat transfer efficiency. This phenomenon enhances fluid mixing and convective currents, leading to improved heat exchange between the nanofluid and the stretching surface. These observations are crucial where optimizing heat dissipation and enhancing thermal performance are critical for efficient energy utilization and system operation.

Table 2 shows (C_f), (*Nu*) and (*Sh*) for various values of (*Nb), (Pr), (Kr), (Sc)* and *(M)* along with a variation in streamwise coordinate value (ξ), *(*$1 \leq \xi \leq 3$). For the *Brownian motion parameter (Nb),* rise in (C_f) with increasing *(Nb)* because of intensified nanoparticle movement haphazardly in nanofluid. This heightened motion increases the interaction between nanoparticles and the fluid, leading to increased surface shear stress thus higher skin friction. Concurrently, the decrease in Nusselt number occurs because enhanced Brownian motion impedes convective heat transfer efficiency. Increased nanoparticle agitation disrupts fluid flow patterns, reducing the effectiveness of convective heat exchange between nanofluid and surface. Similarly, a decrease in (*Sh*) reflects reduced mass transfer rates as increased Brownian motion hinders nanoparticle transport toward the surface. Also, with increasing (*Pr*) and (*M*) values increment in (C_f) and *(Sh*) is driven by the dynamics of thermal and momentum BLs and Lorentz forces. A higher Prandtl number indicates thicker thermal BL and thinner momentum BL due to lower thermal diffusivity relative to momentum diffusivity. Denser thermal BL enhances shear stress, leading to greater (C_f), while thinner momentum BL reduces mass transfer efficiency, resulting in a higher Sherwood number as concentration BL thickens. Conversely, reduction in (*Nu*) reflects reduced convective heat transfer efficiency because of the inhibitive effect of thicker thermal BL. Furthermore, by increasing Schmidt number (*Sc*) and (*Kr*) we observe elevation (C_f), (*Nu*), and (*Sh*) which is due to the impact on fluid viscosity and mass diffusion. A greater concentration boundary layer results from a lower mass diffusivity as compared to momentum diffusivity, as indicated by the Schmidt number and increased resistance to mass transfer. The increased resistance enhances shear stress at the surface, resulting in a higher (C_f). Similarly, the presence of chemical reactions intensifies thermal, and

mass transport processes, leading to higher heat, and mass transfer rates, which elevate (*Nu*), and (*Sh*) respectively. This increases the efficiency of heat and mass transport processes, vital for optimizing various industrial and engineering applications, such as chemical reactors and thermal management systems.

Table 2: Values of *Cf*, *Nu*, and *Sh* for various values of *Nb*, *Kr*, *Pr*, *Sc*, *M* and ξ

Nb	*Kr*	*Pr*	*Sc*	*M*	ξ = 1			ξ = 2			ξ = 3		
					Cf	*Nu*	*Sh*	*Cf*	*Nu*	*Sh*	*Cf*	*Nu*	*Sh*
0.5					-0.2697	-0.1148	0.8499	0.4730	-0.7782	1.1620	1.5700	-2.1182	1.6737
1					-0.2490	-0.1563	0.7824	0.5079	-0.8097	0.9624	1.6169	-2.1286	1.2412
1.5					-0.2306	-0.1882	0.7597	0.5419	-0.8247	0.8956	1.6674	-2.1040	1.0954
2					-0.2141	-0.2117	0.7482	0.5721	-0.8256	0.8620	1.7106	-2.0505	1.0216
2					-0.1863	-0.2377	0.7364	0.6202	-0.7944	0.8282	1.7695	-1.8784	0.9464
	0				-0.2809	-0.1431	0.5237	0.4643	-0.8212	0.7794	1.5734	-2.1880	1.1619
	1				-0.2447	-0.1377	0.9908	0.5086	-0.7821	1.1803	1.6057	-2.0840	1.4887
	2				-0.2310	-0.1319	1.2780	0.5250	-0.7565	1.4380	1.6142	-2.0187	1.7057
	3				-0.2230	-0.1271	1.5046	0.5346	-0.7377	1.6447	1.6181	-1.9720	1.8830
	5				-0.2133	-0.1196	1.8705	0.5464	-0.7108	1.9837	1.6227	-1.9068	2.1795
		1			-0.2570	-0.1409	0.7994	0.4936	-0.7992	1.0124	1.5961	-2.1290	1.3498
		2			-0.2651	-0.3711	0.8741	0.5602	-1.4451	1.2077	1.9086	-3.8392	1.8260
		3			-0.2692	-0.5659	0.9385	0.6142	-1.9983	1.3783	2.1633	-5.5259	2.3139
		5			-0.2666	-0.8925	1.0467	0.7205	-2.9815	1.6827	2.6537	-9.2805	3.4830
		7			-0.2568	-1.1566	1.1336	0.8253	-3.8756	1.9587	3.1505	-14.3484	5.0613
			0.1		-0.3015	-0.1358	0.4311	0.4201	-0.8111	0.6723	1.5030	-2.1409	1.1063
			0.3		-0.2828	-0.1394	0.5645	0.4527	-0.8117	0.7954	1.5486	-2.1550	1.1888
			0.5		-0.2627	-0.1410	0.7400	0.4851	-0.8037	0.9577	1.5876	-2.1403	1.3082
			0.8		-0.2500	-0.1402	0.8803	0.5035	-0.7920	1.0871	1.6046	-2.1100	1.4075
			1		-0.2413	-0.1384	0.9994	0.5151	-0.7797	1.1972	1.6124	-2.0771	1.4948
				0	-0.3074	0.2754	0.6689	0.1212	0.3073	0.6908	0.5169	0.3310	0.7079
				0.1	-0.2880	0.0854	0.7296	0.2628	-0.1255	0.8256	0.8735	-0.4221	0.9363
				0.1	-0.2570	-0.1409	0.7994	0.4936	-0.7992	1.0124	1.5961	-2.1290	1.3498
				0.1	-0.2401	-0.2456	0.8307	0.6297	-1.2042	1.1142	2.1247	-3.6462	1.6665
				0.2	-0.2087	-0.4239	0.8828	0.9155	-2.1079	1.3232	3.5503	-9.1871	2.7575

5. Conclusions:

The following are the findings of the current investigation:

- Apparently elevated (*Nr*) suppresses velocity but enhances temperature and concentration profiles, improving energy and species transport efficiency within the boundary layer due to stronger internal buoyancy forces.
- Evidently higher (*Nt*) values lead to elevated velocity, temperature, and nanoparticle concentration profiles, signifying enhanced momentum, heat, and mass transfer due to the thermophoretic movement of particles from hot to cold regions.
- Predominantly increasing (*Nb*) results in higher velocity and temperature profiles but a decreased nanoparticle concentration profile, indicating improved thermal diffusion and fluid motion, while promoting a more homogeneous nanoparticle distribution. Increasing (*Nb*) raises (C_f) because of intensified nanoparticle interactions but decreases the Nusselt and Sherwood numbers because it disrupts convective heat and mass transfer efficiency.

- Interestingly, boosted (M) values, result in a damped velocity profile due to Lorentz forces opposing fluid motion, while simultaneously elevating temperature and nanoparticle concentration profiles, enhancing thermal energy dispersion and nanoparticle transport. Enhanced (M) reduces (C_f) and (Sh) due to Lorentz forces diminishing frictional resistance and nanoparticle deposition, while improving the Nusselt number by intensifying convective heat transfer through increased fluid mixing.
- Prominently the risen (R) values lead to elevated velocity and temperature profiles, improving heat transfer mechanisms, while nanoparticle concentration decreases due to enhanced thermal energy dissipation.
- Seemingly the heightened (Kr) raises the velocity profile through heat generation and altered fluid properties but decreases temperature and nanoparticle concentration profiles due to energy consumption and changes in fluid dynamics.
- Higher (Kr) boosts (C_f), (Nu) and (Sh) by intensifying thermal and mass transport processes, reflecting improved heat and mass transfer efficiency.
- Indeed greater (Nr) value leads to decreased (C_f) and (Sh) due to opposing buoyancy forces that reduce shear stress and hinder mass transfer while enhancing (Nu) by improving convective heat transfer.
- An intriguing finding is that the higher (Nt) values result in increased (C_f) and (Sh) since the nanoparticle's deposition near the surface, but a decreased Nusselt number because nanoparticle accumulation acts as a thermal barrier, hindering convective heat transfer.
- Improving (R) values, decreases (C_f) and (Sh) by improving heat transmission away from the surface and increases the (Nu) by enhancing convection heat transmission efficiency through intensified fluid mixing and convective currents.
- Significantly, higher (Pr) enhances (C_f) and (Sh) because of thicker thermal and thinner momentum boundary layers, while decreasing the (Nu) to inhibit heat transfer.
- It is noteworthy that, increasing (Sc) elevates (C_f), (Nu) and (Sh) by enhancing fluid viscosity and reducing mass diffusivity, which causes concentration within BL to thicken, and improves shear stress and heat transfer efficiency.

Future scope: Future research on magneto chemically radiative flows of Buongiorno's nanofluid via stretching surface could explore the impacts of different nanoparticle materials and shapes on thermal and mass transmission characteristics. Investigating interaction on various magnetic strengths and orientations with nanofluids can provide insights for optimizing industrial applications. Additionally, extending the study to three-dimensional and turbulent flow regimes can enhance the understanding of complex fluid dynamics. Finally, integrating experimental validation with theoretical models can improve the accuracy and applicability of these findings in real-life scenarios.

Conflicting Interest Disclosure: Writers of this article acknowledge that none of the work reported in this publication could have been influenced by any known conflicting financial interests or interpersonal connections.

Credit authorship contribution statement:

Mrs. Asra Anjum: Conceptualization, Writing an original draft, Drafting, Investigation, and Software. **Dr. Shaik Abdul Gaffar:** Conceptualization, Problem formulation, solving,

Methodology, Software, Supervision. **Dr. D. Sateesh Kumar:** literature survey, editing, Supervision. **Dr**. **O. Anwar Bég:** Editing, Methodology, Conceptualization.

Dr. Samdani Peerusab: Software, editing, Formal analysis.

References

Abbas, A., Jeelani, M. B., Alnahdi, A. S., and Ilyas, A. (2022). MHD Williamson nanofluid fluid flow and heat transfer past a non-linear stretching sheet implanted in a porous medium: effects of heat generation and viscous dissipation. Processes, 10(6), 1221. https://doi.org/10.3390/pr10061221

Ahmad, S., Hayat, T., Alsaedi, A., Ullah, H. and Shah, F. (2021), Computational modeling and analysis for the effect of magnetic field on rotating stretched disk flow with heat transfer, Propuls. Power Res., vol. 10, no. 1, pp. 48–57. https://doi.org/10.1016/j.jppr.2020.11.005

Ashraf M. U., Qasim, M. Wakif, Afridi, M. I. and Animasaun, I. L. (2022), A generalized differential quadrature algorithm for simulating magnetohydrodynamic peristaltic flow of blood-based nanofluid containing magnetite nanoparticles: a physiological, Numer. Methods Partial Differ. Equ., vol. 38, no. 3, pp. 666–692. https://doi.org/10.1002/num.22676.

Basha, H., Thameem, R., Sivaraj, V., Prasad, R. and Beg, O. A. (2021), Entropy generation of tangent hyperbolic nanofluid flow over a circular cylinder in the presence of nonlinear Boussinesq approximation: a non-similar solution, Journal of Thermal Analysis and Calorimetry, 143: 2273-2289. https://dx.doi.org/10.1007/s10973-020-09981-5

Bhavani, J. D., Gopal, T. S., Gnanasekar, S., Pandiaraj, S., Muthuramamoorthy, M., Alodhayb, A. N. and Andrews, N. G. (2024), Ultrasonic Interferometry and Physiothermal properties of Al2O3/CuO nanofluids, Case Studies in Thermal Engineering, 55, 104120. https://doi.org/10.1016/j.csite.2024.104120

Bilal, M., Ramzan, M., (2019), Hall current effect on unsteady rotational flow of carbon nanotubes with dust particles and nonlinear thermal radiation in Darcy-Forchheimer porous media, J. Therm. Anal. Calorim. 138 (5), 3127–3137. https://dx.doi.org/10.1007/s10973-019-08324-3

Buongiorno, J., (2006), Convective transport in Nanofluids, ASME J Heat Trans., Vol. 128, Issue 3, pp.240-250. https://dx.doi.org/10.1115/1.2150834.

Choi, S. U. and J. A. Eastman, (1995), Enhancing thermal conductivity of fluids with nanoparticles, Argonne National Lab. (ANL), Argonne, IL, USA, Tech. Rep. ANL/MSD/CP-84938; CONF-951135-29. OSTI ID:196525

Chu, Y. M., Khan, M. I., Khan, N. B., Kadry, S., Khan, S. U., Tlili, I., and Nayak, M. K. (2020). Significance of activation energy, bio-convection and magnetohydrodynamic in the flow of third-grade fluid (non-Newtonian) towards stretched surface: A Buongiorno model analysis. International communications in heat and mass transfer, 118, 104893. https://dx.doi.org/10.1016/j.icheatmasstransfer.2020.104893

Chu, Y. M., Al-Khaled, K., Khan, N., Khan, M. I., Khan, S. U., Hashmi, M. S., ... and Tlili, I. (2021). Study of Buongiorno's nanofluid model for flow due to stretching disks in the presence of gyrotactic microorganisms. Ain Shams Engineering Journal, 12(4), 3975-3985. https://dx.doi.org/10.1016/j.asej.2021.01.033

Chu, Y. M., Shah, F., Khan, M. I. Kadry, S., Abdelmalek, Z. and Khan, W. A. (2020), Cattaneo-Christov double diffusions (CCDD) in entropy optimized magnetized second-grade nanofluid with variable thermal conductivity and mass diffusivity, J. Mater. Res. Technol., vol. 9, no. 6, pp. 13977–13987. https://doi.org/10.1016/j.jmrt. 2020.09.101.

Ellahi, R., Zeeshan, A., Shehzad, N., and Alamri, S. Z. (2018). Structural impact of Kerosene-Al2O3 nanoliquid on MHD Poiseuille flow with variable thermal conductivity: application of cooling process. Journal of Molecular Liquids, 264, 607-615. https://doi.org/10.1016/j.molliq.2018.05.103

Farooq, U., Hussain, M., and Farooq, U. (2024). Non-similar analysis of micropolar magnetized nanofluid flow over a stretched surface. Advances in Mechanical Engineering, 16(4), 16878132241233089.https://doi.org/10.1177/16878132241233089

Farooq, U., Hussain, M., and Farooq, U. (2024). Non-similar analysis of micropolar magnetized nanofluid flow over a stretched surface. Advances in Mechanical Engineering, 16(4), 16878132241233089. https://doi:10.1177/16878132241233089

Gaffar, S. A., Bég, O. A., Kuharat, S., and Bég, T. A. (2024). Computation of hydromagnetic tangent hyperbolic non-Newtonian flow from a rotating non-isothermal cone to a non-Darcy porous medium with thermal radiative flux. Physics Open, 19, 100216. https://doi.org/10.1016/j.physo.2024.100216

Gaffar, S. A., Prasad, V. R., Bég, O. A., Khan, M. H. H., and Venkatadri, K. (2018). Radiative and magnetohydrodynamics flow of third-grade viscoelastic fluid past an isothermal inverted cone in the presence of heat generation/absorption. Journal of the Brazilian Society of Mechanical Sciences and Engineering, 40, pp 1-19. https://dx.doi.org/10.1007/s40430-018-1049-0

Gaffar, S. A., Prasad, V. R., Reddy, S. K., and Beg, O. A. (2017). Magnetohydrodynamic free convection boundary layer flow of non-Newtonian tangent hyperbolic fluid from a vertical permeable cone with variable surface temperature. Journal of the Brazilian Society of Mechanical Sciences and Engineering, 39, 101-116. https://dx.doi.org/10.1007/s40430-016-0611-x

Gaffar, S. A., Ramachandra Prasad, V., Keshava Reddy, E., and Anwar Bég, O. (2014). Free convection flow and heat transfer of non-Newtonian tangent hyperbolic fluid from an isothermal sphere with partial slip. Arabian Journal for Science and Engineering, 39, 8157-8174.https://dx.doi.org/10.1007/s13369-014-1310-5

Gaffar, S. A., Prasad, V. R., Vijaya, B., and Beg, O. A. (2015). Mixed convection flow of magnetic viscoelastic polymer from a nonisothermal wedge with Biot number effects. International Journal of Engineering Mathematics, 2015(1), 287623. https://dx.doi.org/10.1155/2015/287623

Gireesha, B. J., Umeshaiah, M., Prasannakumara, B. C., Shashikumar, N. S., and Archana, M. (2020). Impact of nonlinear thermal radiation on magnetohydrodynamic three-dimensional boundary layer flow of Jeffrey nanofluid over a nonlinearly permeable stretching sheet. Physica A: Statistical Mechanics and its Applications, 549, 124051. https://doi.org/10.1016/j.physa.2019.124051

Gireesha, B. J., Archana, M., Mahanthesh, B., and Prasannakumara, B. C., (2019), Exploration of activation energy and binary chemical reaction effects on nano Casson fluid flow with the thermal and exponential space-based heat source, Multidiscip. Model. Mater. Struct., 15(1), 227-245. https://dx.doi.org/10.1007/s40819-017-0397-2

Hayat, T., Shah, F., Khan, M. I., Alsaedi, A., and Yasmeen, T. (2017). Modeling MHD stagnation point flow of thixotropic fluid with non-uniform heat absorption/generation. Microgravity Science and Technology, 29, 459-465. https://doi.org/10.1007/s12217-017-9564-7

Hussain, M., Cui, J., Farooq, U., Ahmed Rabie, M. E., and Muhammad, T. (2022). Non-similar modeling and numerical simulations of the electromagnetic radiative flow of nanofluid with entropy generation. Mathematical Problems in Engineering, 2022(1), 4272566. https://doi.org/10.1155/2022/4272566

Humane, P. P., Patil, V. S., Patil, A. B., and Shamshuddin, M. D. (2023). Buongiorno modelled nanoliquid consequence of thermal and solutal convection on the Magneto-micropolar fluid inside an inclined porous stretching device. Journal of Nanofluids, 12(1), 211-222. https://doi.org/10.1166/jon.2023.1949.

Jan, A., Mushtaq, M., Farooq, U., and Hussain, M. (2022). Nonsimilar analysis of magnetized Sisko nanofluid flow subjected to heat generation/absorption and viscous dissipation. Journal of Magnetism and Magnetic Materials, 564, 170153. https://doi.org/10.1016/j.jmmm.2022.170153

Jan, A., Mushtaq, M., Farooq, U., and Hussain, M. (2022). Nonsimilar analysis of magnetized Sisko nanofluid flow subjected to heat generation/absorption and viscous dissipation. Journal of Magnetism and Magnetic Materials, 564, 170153. https://doi.org/10.1016/j.jmmm.2022.170153.

Khan, B. M. H., Gaffar, S. A., Beg, O. A., Kadir, A., and Reddy, P. R. (2020). Computation of Eyring-Powell micropolar convective boundary layer flow from an inverted non-isothermal cone: thermal polymer coating simulation. Computational Thermal Sciences: An International Journal, 12(4). https://doi.org/10.1615/ComputThermalScien.2020033860

Keller, H. B. (1978). Numerical methods in boundary-layer theory. Annual Review of Fluid Mechanics, 10, 417-433.https://doi.org/10.1146/annurev.fl.10.010178.002221

Khan, M. I., Qayyum, S., Kadry, S., Khan, W. A., and Abbas, S. Z. (2020). Irreversibility analysis and heat transport in squeezing nano liquid flow of non-Newtonian second-grade fluid between infinite plates with activation energy. Arabian Journal for Science and Engineering, 45, 4939-4947.https://dx.doi.org/10.1007/s13369-020-04442-5

Khan, W. A., and Pop, I. (2010). Boundary-layer flow of a nanofluid past a stretching sheet. International journal of heat and mass transfer, 53(11-12), 2477-2483. https://doi.org/10.1016/j.ijheatmasstransfer.2010.01

Khechekhouche, A., Manokar, A. M., Sathyamurthy, R., Essa, F. A., Sadeghzadeh, M., and Issakhov, A. (2021). Energy, exergy analysis, and optimizations of collector cover thickness of solar still in El Oued climate, Algeria. International Journal of Photoenergy, 2021(1), 6668325. https://doi.org/10.1155/2021/6668325.

Lee, S., Choi, S. S., Li, S. A., and Eastman, J. A. (1999). Measuring thermal conductivity of fluids containing oxide nanoparticles. Journal of Heat Transfer, vol. 121, no. 2, pp. 280–289. https://doi.org/10.1115/1.2825978

Mahapatra, T. R. R., Pal, D., and Mondal, S. (2012). Influence of thermal radiation on non-Darcian natural convection in a square cavity filled with a fluid-saturated porous medium of uniform porosity. Nonlinear Analysis: Modelling and Control, 17(2), 223-237. https://doi.org/10.15388/NA.17.2.14070.

Nasir, M., Waqas, M., Bég, O. A., Znaidia, S., Khan, W. A., and Zamri, N. (2023). Functional magnetic Maxwell viscoelastic nanofluids for tribological coatings model for stretching flow using the generalized theory of heat-mass fluxes, Darcy-Forchheimer formulation, and dual convection. Tribology International, 187, 108610. https://doi.org/10.1016/j.triboint.2023.108610

Nadeem, S., Ul Haq, R., Akbar, N. S., Lee, C., and Khan, Z. H. (2013). Numerical study of boundary layer flow and heat transfer of Oldroyd-B nanofluid towards a stretching sheet. PloS one, 8(8), e69811. https://doi.org/10.1371/journal.pone.0069811

Prasad, V. R., Gaffar, S. A., Reddy, E. K., and Bég, O. A. (2014). Flow and heat transfer of Jeffreys non-Newtonian fluid from horizontal circular cylinder. Journal of Thermophysics and Heat Transfer, 28(4), 764-770.https://doi.org/10.2514/1.T4253

Razzaq, R., and Farooq, U. (2021). Non-similar forced convection analysis of Oldroyd-B fluid flow over an exponentially stretching surface. Advances in Mechanical Engineering, 13(7), 16878140211034604. https://doi.org/10.1177/16878140211034604

Rasheed, H. U., Islam, S., Khan, Z., Alharbi, S. O., Alotaibi, H., and Khan, I. (2021). Impact of nanofluid flow over an elongated moving surface with a uniform hydromagnetic field and nonlinear heat reservoir. Complexity, 2021(1), 9951162. https://doi.org/10.1155/2021/9951162

Rashid, S., Khan, M. I., Hayat, T., Ayub, M. and Alsaedi, (2020), A. Darcy-Forchheimer flow of Maxwell fluid with activation energy and thermal radiation over an exponential surface, Appl. Nanosci. 10(8), 2965–2975. https://dx.doi.org/10.1007/s13204-019-01008-2

Razzaq, R., Farooq, U., Cui, J., and Muhammad, T. (2021). Non-similar solution for the magnetized flow of Maxwell nanofluid over an exponentially stretching surface. Mathematical Problems in Engineering, 2021(1), 5539542. https://doi.org/10.1155/2021/5539542

Rehman, K. U., Shatanawi, W., and Al-Mdallal, Q. M. (2022). A comparative remark on heat transfer in thermally stratified MHD Jeffrey fluid flow with thermal radiations subject to cylindrical/plane surfaces. Case Studies in Thermal Engineering, 32, 101913. https://doi.org/10.1016/j.csite.2022.101913

Riaz, S., Afzaal, M. F., Wang, Z., Jan, A., and Farooq, U. (2023). Numerical heat transfer of non-similar ternary hybrid nanofluid flow over linearly stretching surface. Numerical Heat Transfer, Part A: Applications, 1-15. https://doi.org/10.1080/10407782.2023.2251093

Ramzan, M., Mohammad, M., Howari, F., Chung, J.D., (2019), Entropy analysis of carbon nanotubes based nanofluid flow past a vertical cone with thermal radiation, Entropy 21 (7), 642. https://dx.doi.org/10.3390/e21070642

Sagheer, S., Razzaq, R., and Vafai, K., (2024), Local non-similar solutions for EMHD nanofluid flow with radiation and variable heat flux along slandering stretching sheet. Numerical Heat Transfer, Part A: Applications, 1–18. https://doi.org/10.1080/10407782.2024.2360082

Sajjad, U., Sadeghianjahromi, A., Ali, H. M., and Wang, C. C. (2020). Enhanced pool boiling of dielectric and highly wet liquids-a review on enhancement mechanisms. International Communications in Heat and Mass Transfer, 119, 104950. https://doi.org/10.1016/j.icheatmasstransfer.2020.104950

Shahid, A., Huang, H. L., Khalique, C. M. and Bhatti, M. M., (2021), Numerical analysis of activation energy on MHD nanofluid flow with exponential temperature-dependent viscosity past a porous plate, J. Therm. Anal. Calorim., 143(3), 2585–259. https://dx.doi.org/10.1007/s10973-020-10295-9

Seyedi, S. H., Saray, B. N. and Chamkha, A. J., (2020), Heat and mass transfer investigation of MHD Eyring-Powell flow in a stretching channel with chemical reactions, Phys. A: Stat. Mech. Appl. 544, 124109. https://dx.doi.org/10.1016/j.physa.2019.124109

Sheikholeslami, M., Sheremet, M. A., Shafee, A., and Li, Z. (2019). CVFEM approach for EHD flow of nanofluid through a porous medium within a wavy chamber under the impacts of radiation and moving walls. Journal of Thermal Analysis and Calorimetry, 138, 573-581. https://dx.doi.org/10.1007/s10973-019-08235-3

Sparrow, E. M., and Yu, H. S. (1971). Local non-similarity thermal boundary-layer solutions. ASME J. Heat Transfer, 93 (4), 328–334.https://doi.org/10.1115/1.3449827

Tlili, I., Samrat, S. P., Sandeep, N., and Nabwey, H. A. (2021). Effect of nanoparticle shape on unsteady liquid film flow of MHD Oldroyd-B ferrofluid. Ain Shams Engineering Journal, 12(1), 935-941.https://doi.org/10.1016/j.asej.2020.06.007

Turkyilmazoglu, M. (2019). MHD natural convection in saturated porous media with heat generation/absorption and thermal radiation: closed-form solutions. Archives of Mechanics, 71(1), 49–64. https://dx.doi.org/10.24423/aom.3049

Vajravelu DK. and K.V. Prasad, (2014), Keller-box method and its application, De Gruyter Studies in Mathematical Physics, De Gruter, USA.

Varatharaj, K., Tamizharasi, R., and Bakar, N. A. (2024). Linear and non-linear stretching surfaces of MHD Casson nanofluid with heat and mass transfer analysis. Mathematical Modelling of Complex Patterns Through Fractals and Dynamical Systems (pp. 77-102). Singapore: Springer Nature Singapore. https://doi.org/10.1007/978-981-97-2343-0_5

Wang, F., Saeed, A. M., Puneeth, V., Shah, N. A., Anwar, M. S., Geudri, K., and Eldin, S. M. (2023). Heat and mass transfer of Ag–H2O nano-thin film flowing over a porous medium: A modified Buongiorno's model. Chinese Journal of Physics, 84, 330-342. https://doi.org/10.1016/j.cjph.2023.01.001.

Yahyaee, A., Hærvig, J., and Sørensen, H. (2024). Nanoparticle migration in nanofluid film boiling: A numerical analysis using the continuous-species-transfer method. International Journal of Heat and Mass Transfer, 224, 125344. https://doi.org/10.1016/j.ijheatmasstransfer.2024.125344.

Zhang, L., Bhatti, M. M., Shahid, A., Ellahi, R., Bég, O. A., and Sait, S. M. (2021). Nonlinear nanofluid fluid flows under the consequences of Lorentz forces and Arrhenius kinetics through a permeable surface: A robust spectral approach. Journal of the Taiwan Institute of Chemical Engineers, 124, 98-105. https://dx.doi.org/10.1016/j.jtice.2021.04.065